sophila diaphanous, is a target protein for Rho small GTPase and is a ligand for profilin. *EMBO J.* **16**, 3044–3056
34. Watanabe, N., Kato, T., Fujita, A., Ishizaki, T., and Narumiya, S. (1999) Cooperation between mDia1 and ROCK in Rho-induced actin reorganization. *Nat. Cell Biol.* **1**, 136–143
35. Tominaga, T., Meng, W., Togashi, K., Urano, H., Alberts, A.S., and Tominaga M. (2002, 2003) The Rho GTPase effector protein, mDia, inhibits the DNA binding ability of the transcription factor Pax6 and changes the pattern of neurite extension in cerebellar granule cells through its binding to Pax6. *J. Biol. Chem.* **277**, 47686–47691; Erratum in: *J. Biol. Chem.* **278**, 17580
36. Tsuji, T., Ishizaki, T., Okamoto, M., Higashida, C., Kimura, K., Furuyashiki, T., Arakawa, Y., Birge, R.B., Nakamoto, T., Hirai, H., and Narumiya S. (2002) ROCK and mDia1 antagonize in Rho-dependent Rac activation in Swiss 3T3 fibroblasts. *J. Cell Biol.* **157**, 819–830
37. Sahai, E. and Marshall, C.J. (2002) ROCK and Dia have opposing effects on adherens junctions downstream of Rho. *Nat. Cell Biol.* **4**, 408–415
38. Kimura, K., Tsuji, T., Takada, Y., Miki, T., and Narumiya, S. (2000) Accumulation of GTP-bound RhoA during cytokinesis and a critical role of ECT2 in this accumulation. *J. Biol. Chem.* **275**, 17233–17236
39. Alberts, A.S. (2002) Diaphanous-related Formin homology proteins. *Curr Biol.* **12**, R796
40. Castrillon, D.H. and Wasserman, S.A. (1994) Diaphanous is required for cytokinesis in *Drosophila* and shares domains of similarity with the products of the limb deformity gene. *Development* **120**, 3367–3377
41. Kohno, H., Tanaka, K., Mino, A., Umikawa, M., Imamura, H., Fujiwara, T., Fujita, Y., Hotta, K., Qadota, H., Watanabe, T., Ohya, Y., and Takai Y. (1996) Bni1p implicated in cytoskeletal control is a putative target of Rho1p small GTP binding protein in *Saccharomyces cerevisiae*. *EMBO J.* **15**, 6060–6068
42. Chang, F., Drubin, D., and Nurse, P. (1997) cdc12p, a protein required for cytokinesis in fission yeast, is a component of the cell division ring and interacts with profilin. *J. Cell Biol.* **137**, 169–182
43. Evangelista, M., Blundell, K., Longtine, M.S., Chow, C.J., Adames, N., Pringle, J.R., Peter, M., and Boone, C. (1997) Bni1p, a yeast formin linking cdc42p and the actin cytoskeleton during polarized morphogenesis. *Science* **276**, 118–122
44. Swan, K.A., Severson, A.F., Carter, J.C., Martin, P.R., Schnabel, H., Schnabel, R., and Bowerman, B. (1998) cyk-1: a *C. elegans* FH gene required for a late step in embryonic cytokinesis. *J. Cell Sci.* **111**, 2017–2027
45. Ozaki-Kuroda, K., Yamamoto, Y., Nohara, H., Kinoshita, M., Fujiwara, T., Irie, K., and Takai, Y. (2001) Dynamic localization and function of Bni1p at the sites of directed growth in *Saccharomyces cerevisiae*. *Mol. Cell. Biol.* **21**, 827–839
46. Narumiya, S. and Mabuchi, I. (2002) Cell biology: spinning actin to divide. *Nature* **419**, 27–28
47. Sagot, I., Klee, S.K., and Pellman, D. (2002) Yeast formins regulate cell polarity by controlling the assembly of actin cables. *Nat. Cell Biol.* **4**, 42–50
48. Evangelista, M., Pruyne, D., Amberg, D.C., Boone, C., and Bretscher A. (2002) Formins direct Arp2/3-independent actin filament assembly to polarize cell growth in yeast. *Nat. Cell Biol.* **4**, 32–41
49. Pruyne, D., Evangelista, M., Yang, C., Bi, E., Zigmond, S., Bretscher, A., and Boone, C. (2002) Role of formins in actin assembly: nucleation and barbed-end association. *Science* **297**, 612–615
50. Sagot, I., Rodal, A.A., Moseley, J., Goode, B.L., and Pellman, D. (2002) An actin nucleation mechanism mediated by Bni1 and profilin. *Nat. Cell Biol.* **4**, 626–631
51. Copeland, J.W. and Treisman, R. (2002) The diaphanous-related formin mDia1 controls serum response factor activity through its effects on actin polymerization. *Mol. Biol. Cell.* **13**, 4088–4099
52. Kovar, D.R., Kuhn, J.R., Tichy, A.L., and Pollard, T.D. (2003) The fission yeast cytokinesis formin Cdc12p is a barbed end actin filament capping protein gated by profilin. *J. Cell Biol.* **161**, 875–887
53. Li, F. and Higgs, H.N. (2003) The mouse formin mDia1 is a potent actin nucleation factor regulated by autoinhibition. *Curr. Biol.* **13**, 1335–1340
54. Evangelista, M., Zigmond, S., and Boone, C. (2003) Formins: signaling effectors for assembly and polarization of actin filaments. *J. Cell Sci.* **116**, 2603–2611
55. Bretscher, A. (2003) Polarized growth and organelle segregation in yeast: the tracks, motors, and receptors. *J. Cell Biol.* **160**, 811–816
56. Gundersen, G.G. and Bretscher, A. (2003) Cell biology. Microtubule asymmetry. *Science* **300**, 2040–2041
57. Rodriguez, O.C., Schaefer, A.W., Mandato, C.A., Forscher, P., Bement, W.M., and Waterman-Storer, C.M. (2003) Conserved microtubule-actin interactions in cell movement and morphogenesis. *Nat. Cell Biol.* **5**, 599–609
58. Ishizaki, T., Morishima, Y., Okamoto, M., Furuyashiki, T., Kato, T., and Narumiya, S. (2001) Coordination of microtubules and the actin cytoskeleton by the Rho effector mDia1. *Nat. Cell Biol.* **3**, 8–14
59. Palazzo, A.F., Cook, T.A., Alberts, A.S., and Gundersen, G.G. (2001) mDia mediates Rho-regulated formation and orientation of stable microtubules. *Nat. Cell Biol.* **3**, 723–729
60. Dent, E.W. and Kalil, K. (2001) Axon branching requires interactions between dynamic microtubules and actin filaments. *J. Neurosci.* **21**, 9757–9769
61. Schaefer, A.W., Kabir, N., and Forscher, P. (2002) Filopodia and actin arcs guide the assembly and transport of two populations of microtubules with unique dynamic parameters in neuronal growth cones. *J. Cell Biol.* **158**, 139–152
62. Vignjevic, D., Yarar, D., Welch, M.D., Peloquin, J., Svitkina, T., and Borisy, G.G. (2003) Formation of filopodia-like bundles in vitro from a dendritic network. *J. Cell Biol.* **160**, 951–962

Cellular/Molecular

Essential Contribution of the Ligand-Binding βB/βC Loop of PDZ1 and PDZ2 in the Regulation of Postsynaptic Clustering, Scaffolding, and Localization of Postsynaptic Density-95

Mio Nonaka,[1,2] Tomoko Doi,[1] Yoshinori Fujiyoshi,[1] Sayaka Takemoto-Kimura,[2] and Haruhiko Bito[2,3]

[1]Department of Biophysics, Kyoto University Graduate School of Science, Kyoto 606-8502, Japan, [2]Department of Neurochemistry, University of Tokyo Graduate School of Medicine, Tokyo 113-0033, Japan, and [3]Solution-Oriented Research for Science and Technology–Japan Science and Technology, Kawaguchi 332-0012, Japan

Postsynaptic density-95 (PSD-95), a PSD-95/Discs large/zona occludens-1 (PDZ) domain-containing scaffold protein, clusters many signaling molecules near NMDA-type glutamate receptors in the postsynaptic densities. Although the synaptic localization of PSD-95 requires palmitoylation of two cysteines at the N terminus and the presence of at least one PDZ domain, how the clustering of PSD-95 is initiated and regulated remains essentially unknown. To address this issue, we examined PSD-95 clustering in primary cultured hippocampal neurons expressing full-length PSD-95 mutant proteins lacking the ligand-binding ability of PDZ1, PDZ2, and/or PDZ3. The formation of either excitatory or inhibitory synapses was unaffected. Combinations of individual mutations, however, significantly reduced the PSD-95 clustering index, in an approximately additive manner. The sensitivity to 2-bromo-palmitate and latrunculin A, reagents known to affect PSD-95 turnover, was also augmented. Furthermore, the synaptic recruitment of a PSD-95 ligand, synaptic GTPase-activating protein (synGAP), was significantly impaired, whereas the clustering of other scaffolding proteins, such as Homer 1c, Shank/Synamon, and PSD-93/Chapsin-110 was spared. Intriguingly, overexpression of the PSD-95 PDZ1/2/3 mutants caused the PSD-95 clusters to localize away from the dendritic shaft, resulting in the formation of elongated spines, in an inverse correlation with the overall PDZ-ligand affinity. Expression of a mutant synGAP lacking the PDZ-binding motif replicated both the clustering and spine morphology phenotypes. In conclusion, the ligand-binding affinity of the PDZ domains of PSD-95, contributed in part via its interaction with the C-terminal end of synGAP, plays a critical role in titrating the synaptic clustering of PSD-95 and controlling its tight association with the PSD scaffold, thereby affecting synapse maturation.

Key words: PSD-95; clustering; spine; synGAP; NMDA receptor; PDZ domains; binding affinity

Introduction

The postsynaptic density (PSD) is an electron-dense structure in which neurotransmitter receptors and associated signaling molecules are tightly clustered. This postsynaptic receptor complex plays an essential role in converting bouts of neurotransmitter release at chemical synapses into postsynaptic electrical and chemical signaling. Knock-in mice expressing a mutant NMDA-type glutamate receptor (NR) subunit 2B, lacking the intracellular C-terminal domain, displayed deficient synaptic properties reminiscent of NR1 knock-out mice (Sprengel and Single, 1999). Therefore, a physical link between the NMDA receptor and the downstream signaling and/or scaffolding molecules appears crucial for establishing normal synaptic function.

A major scaffold protein interacting with the NMDA receptor is PSD-95. This membrane-associated guanylate kinase (MAGUK) superfamily member possesses three N-terminal PSD-95/Discs large/zona occludens-1 (PDZ) domains, a central Src homology 3 (SH3) domain, and a C-terminal guanylate kinase (GK)-like domain (Cho et al., 1992; Kim et al., 1995; Kornau et al., 1995). Different ligand proteins interact with these three class I PDZ domains with various specificities and affinities (Sheng and Sala, 2001). For instance, synGAP (synaptic GTPase-activating protein) (Chen et al., 1998; Kim et al., 1998) binds to each PDZ equally. In contrast, the C-terminal PDZ-binding motif (–ESDV) of the NR2 subunit binds to PDZ1 and PDZ2 (Kornau et al., 1995), whereas ligands such as neuroligin (Irie et al., 1997) and cysteine-rich interactor of PDZ3 (CRIPT) (Niethammer et al., 1998) preferentially interact with PDZ3.

Extensive deletion mutagenesis studies established that the clustering of PSD-95 involves multimerization mediated by the

Received June 17, 2005; revised Nov. 18, 2005; accepted Nov. 22, 2005.

This work was supported by grants-in-aid from the Ministry of Education, Culture, Sports, Science, and Technology of Japan (Y.F., H.B.) and by grants from the Human Frontier Science Program, Solution-Oriented Research for Science and Technology–Japan Science and Technology, and the Ministry of Health, Labor, and Welfare of Japan (H.B.). We thank Dr. Yutaka Hata (Tokyo Medical and Dental University, Tokyo, Japan) for providing the Shank antibody, Dr. Hideru Togashi (Center for Developmental Biology, RIKEN, Kobe, Japan) for assistance with low-density rat primary culture and electroporation techniques, and Dr. Toshifumi Tomoda (City of Hope National Medical Center, Beckman Research Institute, Duarte, CA) and Dr. Richard L. Huganir (Johns Hopkins University, Baltimore, MD) for the synGAP cDNAs. We also thank Dr. Makoto Goda for assistance with the light microscopy systems, Ayako Tanaka for cloning the CRIPT cDNA, Taichi Okamoto for technical assistance, and Dr. Hiroyuki Okuno for discussions on statistical data analysis.

Correspondence should be addressed to Tomoko Doi, Department of Biophysics, Kyoto University Graduate School of Science, Kitashirakawa-oiwake, Sakyo, Kyoto 606-8502, Japan. E-mail: doi@em.biophys.kyoto-u.ac.jp.

DOI:10.1523/JNEUROSCI.2489-05.2006

 0270-6474/06/260763-12$15.00/0

N-terminal region containing palmitoylated Cys-3 and Cys-5, and that the presence of one PDZ domain is sufficient for its synaptic targeting (Craven et al., 1999; Hsueh and Sheng, 1999; Christopherson et al., 2003). The importance of the tandem order of PDZ domains and of the short linker between them has also been suggested (Long et al., 2003). Furthermore, the PDZ-ligand interactions probably trigger and promote clustering via intermolecular interactions through the SH3–GK domains (Brenman et al., 1998; McGee et al., 2001; Tavares et al., 2001). However, the individual contribution of each PDZ domain and the impact of the series of ligand-binding sites on the clustering and scaffolding functions of PSD-95 have not been quantitatively examined.

To address these questions, we used PSD-95 mutants with an intact overall protein length and domain structure, in which specific mutations were introduced at the ligand-binding βB/βC loop of the PDZ1 and/or PDZ2 domains (Imamura et al., 2002). These PDZ1/2 ligand-binding site mutants were further combined with the N326S mutation in PDZ3, which greatly reduces the PDZ3–ligand affinity (Niethammer et al., 1998). By overexpressing these PSD-95 mutants with either individual or combined PDZ mutations in cultured hippocampal neurons, we probed the contributions of the individual ligand-binding sites in the clustering, membrane anchoring, and scaffolding functions of PSD-95. Our results suggested that multivalent ligand binding via the βB/βC loops of PDZ1 and PDZ2, in part by interacting with synGAP, not only plays a critical role in titrating the synaptic clustering and anchoring of PSD-95 but also, surprisingly, contributes to attracting the PSD-95-based scaffold to the proximity of dendritic shafts during synapse maturation.

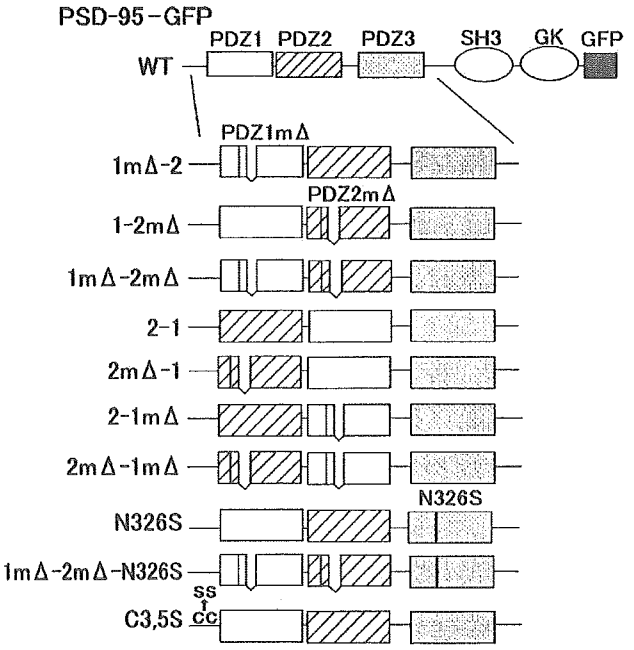

Figure 1. Schematic diagram of the domain structures of the series of PSD-95–GFP mutants and the wild type. The top panel shows the domain structure of PSD-95 tagged with GFP at the C terminus. The mutant illustrations show the N-terminal segment of PSD-95, including only the PDZ domains. PDZ1mΔ and PDZ2mΔ represent the PDZ1 and PDZ2 domains, respectively, with deletions of six amino acids (intervals) and point mutations that abolished their ligand-binding activity. The PDZ3 domain with the N326S point mutation (black vertical bar) has weak ligand-binding activity.

Materials and Methods

DNA constructs. The mutated PSD-95 cDNAs were constructed as described previously (Imamura et al., 2002). These were fused to enhanced green fluorescent protein (EGFP) via a linker sequence, Gly-Gly-Gly-Ser, using PCR in the EGFP-N1 vector (BD Biosciences-Clontech, Palo Alto, CA). The C3,5S and N326S mutations were introduced using a Quikchange mutagenesis kit (Stratagene, La Jolla, CA). The pRK5-synGAP(TRV) cDNA tagged with N-terminal Myc was obtained from Toshifumi Tomoda (City of Hope National Medical Center, Beckman Research Institute, Duarte, CA) with permission from Richard Huganir (Johns Hopkins University, Baltimore, MD), and mutagenesis was performed by PCR. All constructs were confirmed by DNA sequencing.

Primary culture, transfection, and immunocytochemistry. For immunocytochemical analyses, we prepared primary cultures of hippocampal neurons from either ICR mice or Wister rats, purchased from Japan SLC (Shizuoka, Japan). The high-density primary culture from postnatal days 0 to 1 mouse hippocampus was performed as described previously (Furuyashiki et al., 2002). Briefly, 4×10^4 cells were plated onto Matrigel (BD Biosciences, Bedford, MA)-coated spots of ~5 mm in diameter on glass coverslips, and the cultured neurons were fed with fetal calf serum-containing medium in the presence of Ara-C (Sigma, St. Louis, MO). Cultured neurons were transfected at 9 d *in vitro* (DIV) using the calcium phosphate method (Takemoto-Kimura et al., 2003), and then the cells were fixed at 12 DIV. In cotransfection experiments examining the effect of overexpressing wild-type (WT) or mutant synGAP, neurons were transfected at 8 DIV by lipofection using Lipofectamine 2000 (Invitrogen, Carlsbad, CA), and cell phenotypes were examined at 10 DIV.

For immunocytochemistry, neurons were fixed in PBS(−) containing 4% paraformaldehyde/4% sucrose (or 2% paraformaldehyde/4% sucrose for PSD-93 staining). Fixed neurons were quenched in 0.1 M glycine/PBS(−), permeabilized with 0.2% Triton X-100/PBS for 10 min on ice, thoroughly washed with PBS(−), incubated in blocking solution [3% BSA/PBS(−)] for 30 min at room temperature, and then incubated overnight with primary antibodies (listed below) diluted in the blocking buffer at 4°C. The next day, the neurons were washed three times with PBS(−) and then were incubated with Alexa Fluor-conjugated secondary antibodies (Invitrogen) at a 1:500 dilution in blocking buffer. The antibody sources and dilutions are as follows: rabbit polyclonal anti-vesicular glutamate transporter-1 (VGLUT1) (1:1000; Synaptic Systems, Goettingen, Germany), monoclonal anti-vesicular GABA transporter (VGAT) (1:1000; Synaptic Systems), monoclonal anti-synaptophysin (1:1000; Sigma), monoclonal anti-PSD-95 [K28/43, 1:200 (Upstate Biotechnology, Lake Placid, NY); 7E3–1B8, 1:250 (Affinity BioReagents, Golden, CO)], monoclonal anti-synGAP (1:1000; Affinity BioReagents), rabbit polyclonal anti-Homer-1c (Irie et al., 2002), rabbit polyclonal anti-PSD-93 (1:250; Zymed, San Francisco, CA), rabbit polyclonal anti-Synamon/Shank (a kind gift from Yutaka Hata, Tokyo Medical and Dental University, Bunkyo-ku, Tokyo, Japan), polyclonal anti-Myc (1:200; Cell Signaling Technology, Beverly, MA), and Alexa Fluor-conjugated anti-rabbit and anti-mouse antibodies (1:500; Invitrogen).

Pharmacological treatments. Pharmacological treatments were performed by low-density rat hippocampal cultures, and the resulting effects were examined by immunofluorescent (IF) staining, as described previously (Togashi et al., 2002). The PSD-95 mutant phenotypes reported in this study were essentially identical, regardless of the type of primary culture (data not shown). At 12 or 13 DIV, one-half of the culture medium was removed from the dish, and 2-bromo-palmitate (2-Br-Pal) or latrunculin A (LatA) (from a 1000× stock in DMSO) were mixed with this half, to concentrations of 200 and 10 μM, respectively. This medium was then returned to the culture dish and mixed well with the remaining medium by gentle rocking. After either a 2 or 8 h treatment, the cells were washed with cold PBS(−) and fixed immediately. Latrunculin A was obtained from Calbiochem (La Jolla, CA), and 2-Br-Pal (2-bromohexadecanoic acid) was from Sigma.

Quantitative microscopy and image analysis. All immunofluorescence images were acquired using a cooled CCD camera (Orca II; Hamamatsu Photonics, Hamamatsu, Shizuoka, Japan), controlled by the MetaVue or MetaMorph software (Molecular Devices, Sunnyvale, CA) and mounted on either a BX50 upright or an IX-81 inverted microscope (Olympus Optical, Tokyo, Japan) with 100× [numerical aperture (NA), 1.35] and

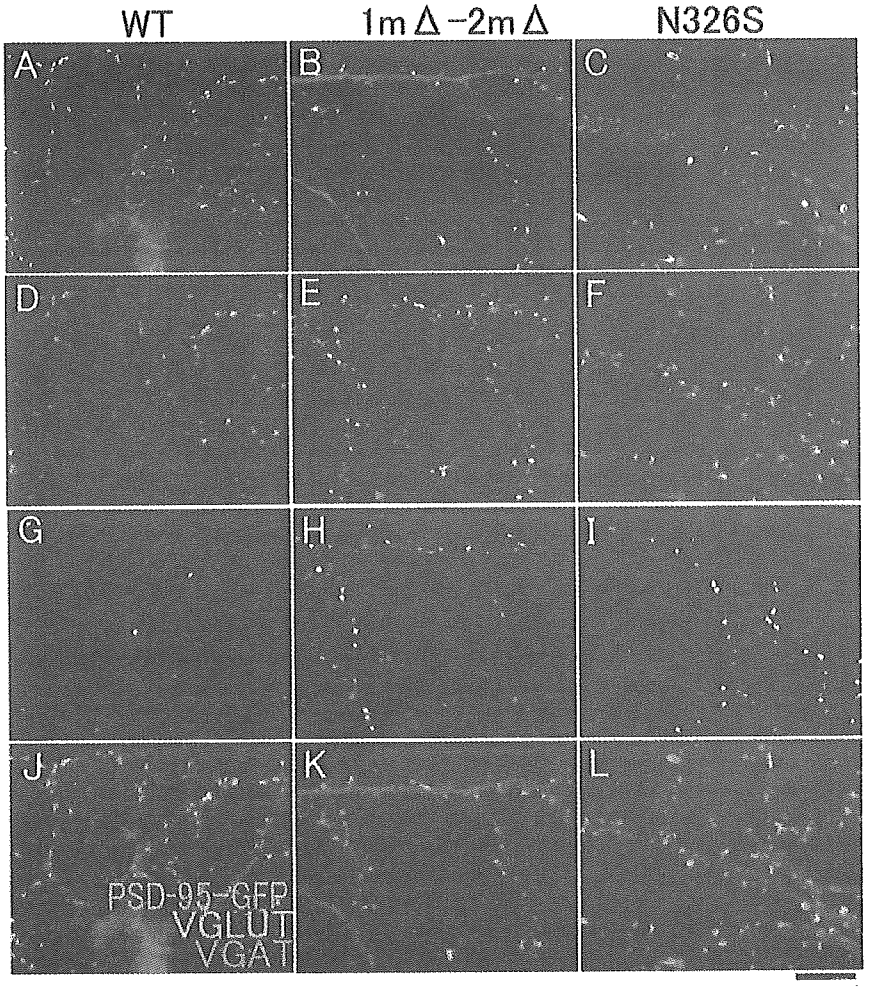

Figure 2. Wild-type and mutant PSD-95 form postsynaptic clusters apposed to the glutamatergic synaptic boutons. The PSD-95(WT)–GFP, 1mΔ-2mΔ, and N326S (***A–C*** and green in ***J–L***, respectively) form clusters juxtaposed to puncta immunopositive for an excitatory presynaptic marker, anti-VGLUT1 (***D–F*** and red in ***J–L***). No cluster colocalized with puncta positive for an inhibitory presynaptic marker, anti-VGAT (***G–I*** and blue in ***J–L***). The bottom images are merged images in which PSD-95–GFP staining is green, VGLUT1 staining is red, and VGAT staining is blue. Scale bar, 10 μm.

40× (NA, 0.85) objectives and filter cubes appropriate for costaining of GFP, Alexa 594, and Alexa 350, or GFP, Alexa 555, and Alexa 647. Immunostaining and image acquisition were performed using rigorously identical procedures within a set of experiments, which enabled us to obtain reproducible sets of immunofluorescence values, as detected by the cooled CCD camera.

For quantification purposes, only the neurons that expressed PSD-95–GFP within the average intensity values of 100–300 (in a 12-bit dynamics range, 0–4096 at a fixed gain setting) in the dendritic shafts were considered and randomly chosen, because most of the cells with normal morphology fell within this value range. In the preliminary series of experiments, the minimum and maximum intensity values, 100 and 300, were set as reliable thresholds to obtain a sufficient amount of mutant proteins to reveal a dominant phenotype and to avoid the toxic effects attributable to the overexpression of exogenous proteins, respectively. For each cell, one to four images were acquired to cover the main dendritic area. The dendritic segments (the apparent dendritic shaft diameter was >0.7 μm) were chosen randomly within 200 μm from the soma. For the synaptic clustering index (SCI), cluster density (the number of clusters per 20 μm dendritic segment), and cluster-shaft distance measurements, the PSD-95 clusters were defined as 0.3–1.0 μm diameter spots of increased GFP fluorescence, at least twice as bright as the dendritic shaft (to discriminate true clusters from stochastic local gradients; however, because of spatial resolution limitations, we were unable to reliably resolve clusters less than ~0.2 μm in diameter), which were closely juxtaposed to synaptophysin-immunopositive puncta. In the obtained ensemble dataset, both the cluster size and average cluster fluorescence intensity followed a Gaussian distribution, indicating that no systematic bias was introduced by these criteria.

The SCI was calculated off-line with the MetaVue or MetaMorph software, essentially as described previously (Arnold and Clapham, 1999), using images acquired with the 100× (NA, 1.35) objective. Briefly, after subtracting the background, the maximal intensity of each synaptic cluster was divided by the average intensity of the proximal parent dendritic shaft. The average dendritic shaft intensity was measured by drawing an orthogonal line traversing the dendritic area immediately nearest/adjacent to the cluster but excluding any outlying bright spots. Because we used wide-field microscopy, the inclusion of immunofluorescence values obtained from out-of-focus fields would inevitably result in underestimation and inexact SCI values. To avoid this, we determined the in-focus area of interest within each image and only analyzed the immunofluorescence values obtained from dendrites and clusters located within that area. In control experiments, the SCI analysis performed over the same fields of view, using a 40× objective lens, yielded quantitatively similar results, confirming that under our experimental conditions, the contribution of the out-of-focus photons was negligible, even with the 100× (NA, 1.35) objective (data not shown).

For the cluster-shaft distance measurement, the images were displayed at the same magnification, and the synaptic clusters were chosen using the same criteria as for the SCI measurement. A line was manually drawn off-line from the center of each synaptic cluster to the nearest edge of their parent dendritic shafts, and the length was measured using the MetaVue or MetaMorph software. A distance value of zero was applied to those clusters formed directly on the dendritic shaft (shaft clusters). We acknowledge the caveat that such data obtained from projection images strongly underestimate the protrusion into the *z*-axis but this does not alter the main results of our analyses, because this *z*-axis underestimation factor is equally distributed across the *x–y* plane, although the correlation factor obtained in Figure 7*A* may be slightly underrepresented.

The SCI and cluster-shaft distance values were thus calculated for 20–100 clusters from at least 100 μm of dendritic segments per cell, and the average values for each cell were further subjected to a multicomparison analysis. Six to 11 cells were analyzed in total for each individual PSD-95 mutant construct. For the statistical analysis, the SCI measurement was evaluated by one-way ANOVA, with the *post hoc* Dunnett's test, using the JMP software (SAS Institute, Toronto, Ontario, Canada), and the cumulative distribution of the cluster-shaft distances was analyzed by the Kolmogorov–Smirnov test, using the PAST software (Hammer et al., 2001). Graphs were made with the Prism software (GraphPad Software, San Diego, CA) and Excel (Microsoft, Seattle, WA).

Results

Construction of full-length PSD-95 mutants containing PDZ domains with reduced binding affinity

The mutant PDZ domains, PDZ1mΔ and PDZ2mΔ, in which the ligand-binding βB/βC loop of either the PDZ1 or PDZ2 domain

of PSD-95 was altered, were shown previously to be unable to bind to NR2B and Kv1.4, both *in vitro* and in a heterologous system (Imamura et al., 2002). We further confirmed that they are also unable to bind CRIPT, a well known neuronal PDZ3 ligand, despite the apparent homology between the mutated PDZ1/2 sequences and PDZ3 (supplemental Fig. 1, available at www.jneurosci.org as supplemental material). To further disrupt the ligand binding at the PDZ3 domain, we introduced an additional point mutation, N326S (Niethammer et al., 1998). This significantly reduced the binding of mutated PDZ3 to CRIPT and allowed only weak binding to Kv1.4 (supplemental Fig. 1, available at www.jneurosci.org as supplemental material). Based on these results, we next systematically replaced the PDZ1, PDZ2, and PDZ3 of PSD-95 with PDZ1mΔ, PDZ2mΔ, and PDZ3 (N326S) and fused EGFP at their respective C termini. Figure 1 shows the series of PSD-95–GFP mutants used in this study. The PDZ1–PDZ2 inverted mutants were also constructed to test whether the relative positions of the PDZ domains were as important in cultured neurons as in a heterologous expression system (Imamura et al., 2002).

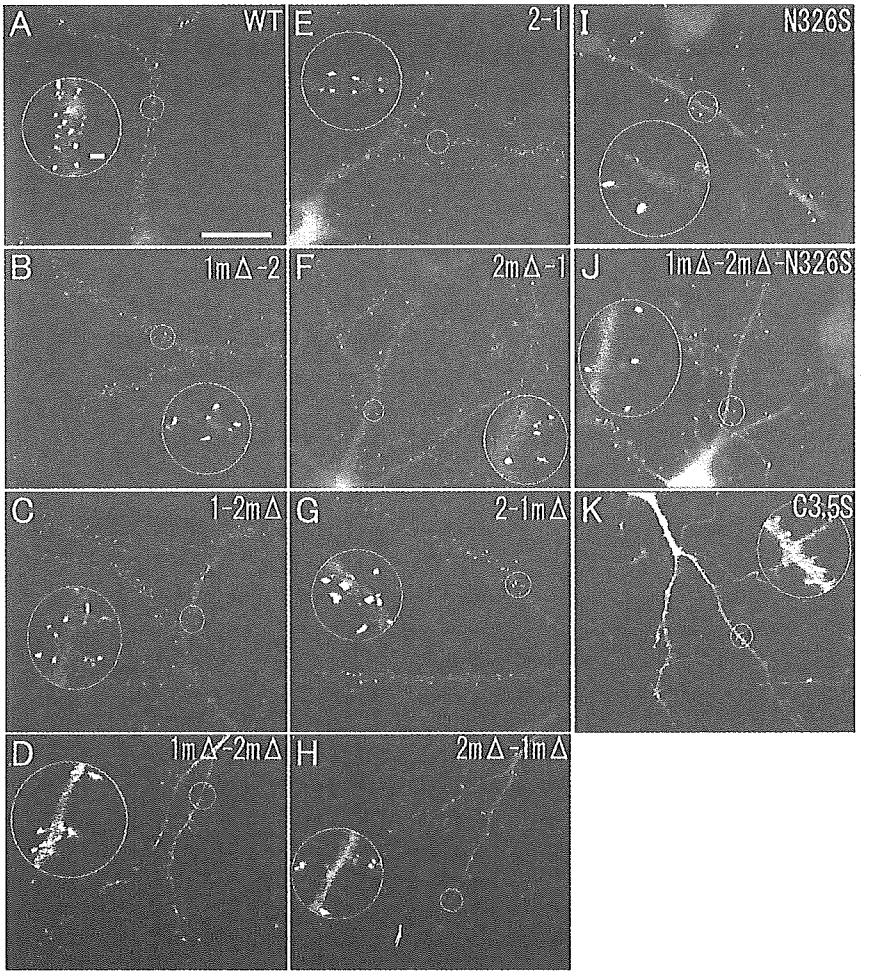

Figure 3. Synaptic clustering of PSD-95 is diminished by PDZ-ligand-binding mutations. GFP fluorescent images were taken from transfected hippocampal neurons expressing the wild-type (*A*) and the series of mutant PSD-95–GFPs (*B–K*). *A*, *E*, The wild-type and the 2–1 (inversion of PDZ1 and PDZ2, with intact ligand-binding affinity) mutant formed bright shaft clusters. Note that the majority of the clusters are shaft clusters. *B*, *C*, *F*, *G*, When either the PDZ1 or PDZ2 domain is mutated, the clustering activity is slightly reduced. A significant number of clusters are formed at some distance from the dendritic shaft, indicating their presence on spine-like protrusions. *D*, *H*, Mutations in both PDZ1 and PDZ2 reveal clusters located farther away, on the tips of longer protrusions. In contrast to the WT, the fluorescence intensity of these clusters is not substantially higher compared with the mean dendritic shaft intensity. *I*, The N326S mutation in the PDZ3 domain also reduces the clustering efficiency. *J*, 1mΔ–2mΔ–N326S, the mutant that lacks functional PDZ domains, forms discernible clusters juxtaposed to the presynaptic markers, but the clustering efficiency is extremely low. The clusters are even farther from their parent dendritic shafts. All of the ligand-binding-deficient mutants are distinct from the C3,5S mutant (*K*) in that they form punctate clusters. Scale bars: 20 μm; inset, 1 μm. The insets are the magnified images of the areas outlined by white circles in the images. All of the insets have the same magnification.

Individual PDZ domains independently and additively contribute to the synaptic clustering of PSD-95

To examine the role of ligand binding to each individual PDZ domain in postsynaptic clustering during synaptic maturation, we transfected the cDNAs for each PSD-95–GFP mutant in cultured mouse hippocampal neurons at 9 DIV. Neurons were fixed at 12 DIV and immunostained with a presynaptic marker. We first confirmed that exogenous PSD-95(WT)–GFP and PSD-95(1mΔ–2mΔ)–GFP formed clusters in puncta of ~0.3–0.4 μm in diameter. These PSD clusters were juxtaposed to puncta immunoreactive to VGLUT1, a marker for excitatory glutamatergic termini, but were far from puncta immunoreactive to VGAT, a marker for inhibitory GABAergic termini (Fig. 2). We initially calibrated the expression levels of the PSD-95–GFP constructs by comparing the anti-PSD-95-immunoreactive signals of untransfected neurons with those of transfected neurons containing both exogenous and endogenous PSD-95. We established that, at a fixed gain setting, using our cooled CCD acquisition system, neurons with mean GFP intensities in dendritic shafts between 100 and 300 had a dendritic morphology indistinguishable from that of untransfected neurons. The anti-PSD-95 immunoreactivity completely overlapped with the GFP puncta, and the GFP fluorescence intensities of 100–300 corresponded to ~3.4- to 5.6-fold higher amounts of PSD-95 immunoreactivity compared with the basal, endogenous levels in untransfected cells. In the mutant PSD-95–GFP containing PDZ1mΔ, the distribution of endogenous PSD-95, stained using a PSD-95 antibody (7E3–1B8) that did not recognize the PDZ1mΔ, was indistinguishable from the GFP fluorescence from the mutant PSD-95 molecules (data not shown). Furthermore, we confirmed that the overexpression of the full-length wild-type or mutant PSD-95–GFP constructs in neurons apparently had minimal effects on the integrity of the full-length protein (supplemental Fig. 2, available at www.jneurosci.org as supplemental material). The wild-type and mutant PSD-95–GFP were able to form complexes when expressed in COS cells, because they coimmunoprecipitated together (data not shown). Thus, the exogenously expressed PSD-95–GFP freely intermingled with the endogenous PSD-95. Therefore, any phenotypic change resulting from overexpressing the mutant PSD-95, as opposed to overexpressing the wild-type PSD-95, was likely to result from a dominant effect triggered by the reduced binding affinity of the mutated PDZ domain(s).

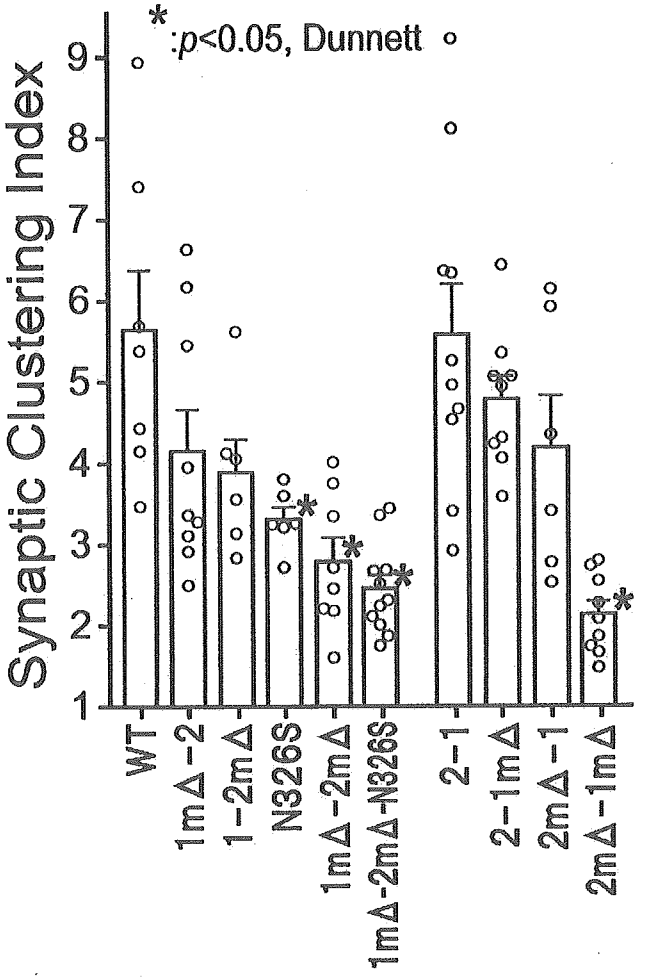

Figure 4. Individual PDZ domains independently and additively contribute to postsynaptic clustering of PSD-95. The SCI was measured as the peak GFP intensity of the synaptic PSD-95–GFP clusters divided by the average intensity of the parent dendritic shaft. Wild-type PSD-95 forms clusters that are 5.64 ± 0.73 times as bright as the parent dendritic shaft, on average. In contrast, the 1mΔ–2mΔ mutant forms clusters with an SCI of approximately half of the wild type (SCI, 2.79 ± 0.298; $p < 0.05$ vs WT). Open bars and error bars are means ± SEM of the cell averages ($n = 6$–11 cells), and open circles represent the average of each cell (20–100 clusters per cell). We confirmed that the SCI values of each cluster in a cell conformed to a normal distribution. Each dataset was statistically analyzed by one-way ANOVA, with the *post hoc* Dunnett's test. *$p < 0.05$ versus WT.

To quantitatively measure the clustering efficiency at the postsynaptic site, we used the SCI (Arnold and Clapham, 1999). Basically, the SCI was calculated as the peak GFP pixel intensity at the clusters juxtaposed to the presynaptic markers divided by the average GFP pixel intensity of the adjacent dendritic shaft (see Materials and Methods). The SCI value varied from cluster to cluster and cell to cell, but the values exhibited a normal distribution (data not shown). The average SCI of the wild type was 5.64 ± 0.73 (mean ± SEM) (Figs. 3*A*, 4). The C3,5S mutant, which lacks the two palmitoylation sites at the N terminus, was localized diffusely (Fig. 3*K*), as reported previously (Craven et al., 1999). In contrast to the C3,5S mutant, all of the ligand-binding-deficient mutants formed distinguishable clusters (Fig. 3*B–J*) juxtaposed to the presynaptic marker synaptophysin. However, the synaptic clusters of these mutants were less dense, with a substantial portion of the PSD-95–GFP molecules remaining unclustered in dendritic shafts (Fig. 3*D,H,J*). Noticeable degradation of the PSD-95–GFP proteins in transfected neurons overexpressing either the wild-type or mutant PSD-95–GFP proteins was not detected (supplemental Fig. 2, available at www.jneurosci.org as supplemental material), indicating that the loss of synaptic clustering probably resulted from dispersion rather than protein degradation. The postsynaptic clustering activity was significantly attenuated in the 1mΔ–2mΔ mutant compared with the wild type (Fig. 4) (SCI, 2.79 ± 0.30; $p < 0.05$, ANOVA with the *post hoc* Dunnett's test). The N326S mutation in PDZ3 also significantly reduced the clustering efficiency (SCI, 3.18 ± 1.87; $p < 0.05$, ANOVA with the *post hoc* Dunnett's test), to an extent approximately comparable with that of the 1mΔ–2mΔ mutant. These results suggested that synaptic clustering is not only governed by ligand binding to the PDZ3 domain, whose contribution was shown previously in a peptide inhibition experiment (Passafaro et al., 1999), but also by ligand binding to both PDZ1 and PDZ2. Consistent with this idea, the 1mΔ–2mΔ–N326S mutant exhibited the lowest clustering efficiency of all of the non-inverted mutants (SCI, 2.44). The inversion of the mutated PDZ domains had no discernable effect per se on synaptic clustering in hippocampal neurons ($SCI_{2mΔ-1}$, 4.19 ± 0.64, $SCI_{2-1mΔ}$, 4.78 ± 0.28 vs $SCI_{1mΔ-2}$, 4.15 ± 0.51, $SCI_{1-2mΔ}$, 3.89 ± 0.40), unlike the results seen previously in a heterologous expression system with only Kv1.4 as a ligand (Imamura et al., 2002). This probably reflects the complexity of the stoichiometry and the competition among multiple PDZ ligands for PSD-95 binding within the small volume of the PSD near physiological synapses.

Collectively, these observations support the notion that the ligand binding to PDZ1, PDZ2, and PDZ3 independently contributes to the postsynaptic clustering of PSD-95 at the PSD, and that this regulation operates in an approximately additive manner.

Postsynaptic clustering of a PSD-95 ligand, synGAP, is severely altered in PSD-95 mutant expressing neurons, but the clustering of Shank/Synamon, Homer, and PSD-93 remains intact

We next tested whether a loss in PDZ binding affinity in PSD-95 affected the recruitment of a nontransmembrane PDZ ligand or PSD scaffolds distinct from PSD-95 by performing immunocytochemical analyses in synaptic clusters of wild-type and mutant expressing neurons. We found no significant difference in the immunoreactivity (IF) intensity at synaptic clusters for either Shank/Synamon, Homer 1c/Vesl-L/PSD-Zip45, or PSD-93/Chapsin-110, three postsynaptic molecular scaffold proteins distinct from PSD-95, between the neurons expressing wild-type PSD-95 and the 1mΔ–2mΔ mutant ($p > 0.5$ in all IF experiments) (Fig. 5*C–E*). In contrast, the staining intensity for synGAP, a major PSD-95 ligand, was significantly reduced in the neurons expressing the 1mΔ–2mΔ and 1mΔ–2mΔ–N326S PSD-95 mutants compared with the wild-type expressing neurons (Fig. 5*A,B1,B2*) [mean ± SEM; WT, 2.88 ± 0.20; 1mΔ–2mΔ, 1.9 ± 0.17; $p < 0.05$ (*t* test) vs WT; and WT, 3.4 ± 0.62; 1mΔ–2mΔ–N326S, 1.7 ± 0.12; $p < 0.05$ (*t* test) vs WT]. These results suggest that the impact of the reduced PDZ-ligand affinity of PSD-95 is limited to the primary PSD-95 ligands and may not extend to other PSD proteins indirectly associated with PSD-95 via the scaffolding complexes present in the PSD.

Loss of the ligand-binding affinity in PDZ domains destabilizes the PSD-95 association with the PSD

Previous work examining PSD-95 turnover at and near synapses demonstrated that only a limited pool of PSD-95 undergoes active turnover (Okabe et al., 1999), and an EM study further suggested that PSD-95 is deeply anchored to the core fraction (<12 nm from the postsynaptic membrane) of the PSD (Petersen et al., 2003). To investigate whether the PDZ-ligand binding plays a role in the tight integration of PSD-95 in the PSD, we treated neurons with 100 μM 2-bromo-palmitate, a reagent that blocks palmitoylation (El-Husseini Ael et al., 2002) and thereby inhibits the delivery of PSD-95 to plasma membranes. Within 2 h after treatment, the synaptic clustering of PSD-95 in the wild-type expressing neurons, measured using SCI, only decreased by 14.2% compared with the vehicle-treated control, whereas the SCI in the mutant (1mΔ–2mΔ) PSD-95 expressing neurons significantly decreased to almost half of that of the control (55.7%; $p < 0.01$, Student's t test) (Fig. 6*A*). After an 8 h incubation, the SCI values of the wild-type expressing neurons were reduced to a level similar to that of the 1mΔ–2mΔ mutant. Thus, the removal of PSD-95 from the synaptic clusters was facilitated in the 1mΔ–2mΔ mutant as a result of the reduced delivery of new palmitoylated PSD-95 to the surface membranes. This result suggests that intact PDZ1/2 ligand binding may contribute to synaptic clustering by either promoting the aggregation of palmitoylated PSD-95 molecules or facilitating the maintenance of the palmitoylated form of PSD-95.

We then tested the PSD-95 mutants for a potential alteration in the susceptibility of postsynaptic clustering to 5 μM LatA, a reagent that favors filamentous actin (F-actin) depolymerization within spines (Allison et al., 1998). In the wild-type PSD-95 expressing neurons, LatA treatment for 17 h was required to substantially reduce the SCI. Even after 17 h of treatment, distinct clusters remained on dendrites ($SCI_{0\ h}$, 6.31 ± 0.30; $SCI_{17\ h}$, 4.12 ± 0.20; $p' < 0.01$) (Fig. 6*B*). In contrast, in the 1mΔ–2mΔ mutant expressing neurons, the clusters readily dissociated within 1.5 h ($SCI_{0\ h}$, 3.63 ± 0.086; $SCI_{1.5\ h}$, 2.61 ± 0.23; $p < 0.01$). However, when scaled to the untreated cells, the SCI values of the wild-type and 1mΔ–2mΔ expressing neurons both decreased, to 65.3 and 61.8% of the original levels, respectively, after 17 h of treatment. Therefore, similar to the

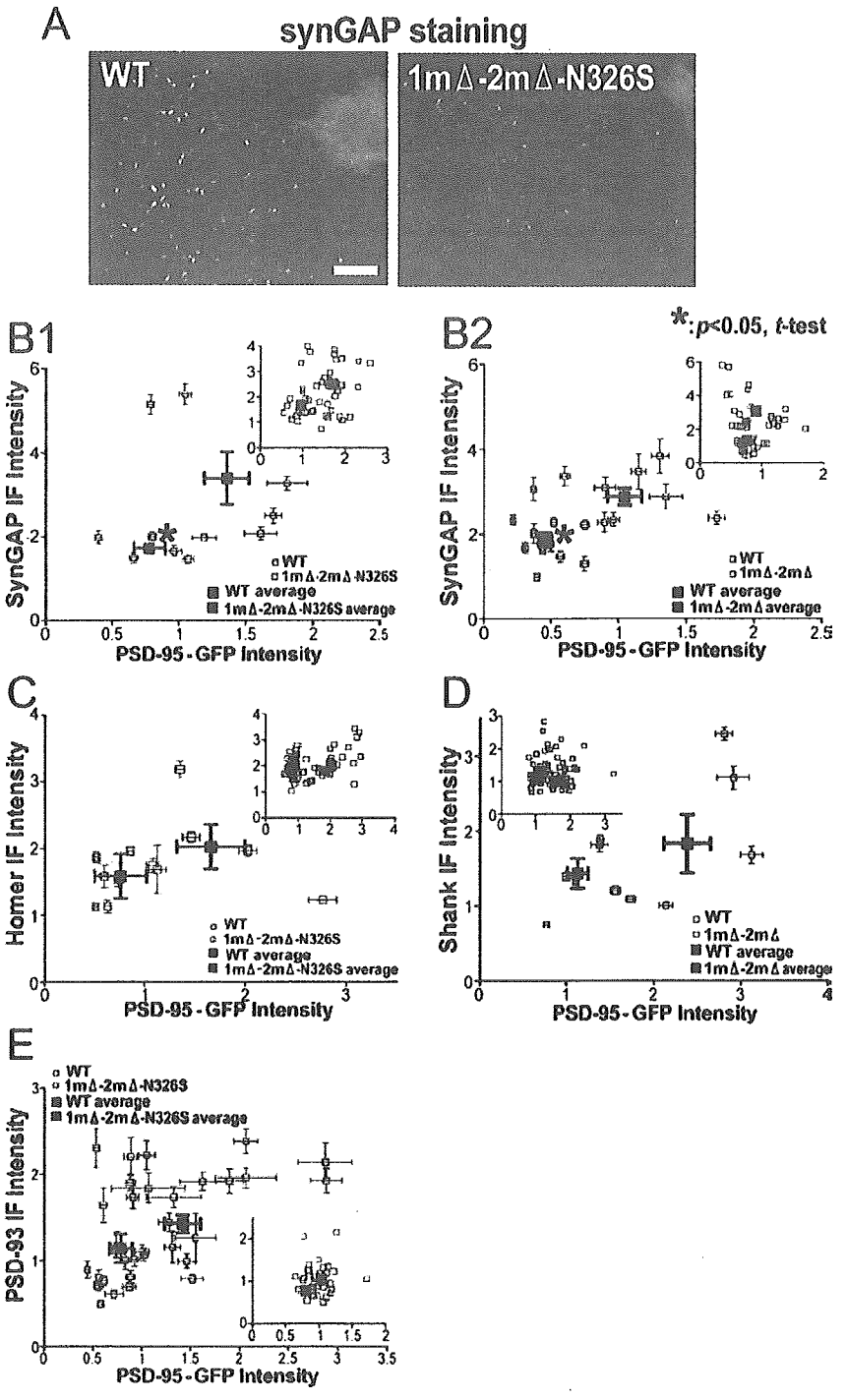

Figure 5. SynGAP immunoreactivity is significantly reduced in the postsynaptic clusters of 1mΔ–2mΔ PSD-95-expressing neurons compared with the wild-type PSD-95-expressing neurons. ***A***, SynGAP IF images of the cells expressing PSD-95(WT)–GFP and 1mΔ–2mΔ–N326S are shown in grayscale. The staining signal is significantly reduced in the postsynaptic clusters of the 1mΔ–2mΔ PSD-95-expressing neurons compared with the wild-type PSD-95-expressing neurons. Scale bar, 10 μm. ***B–E***, Graphs represent the plots of the IF intensities of synGAP (***B***), Homer (***C***), Shank (***D***), and PSD-93 (***E***) versus the PSD-95–GFP intensities of the clusters in the neurons expressing wild-type or mutant PSD-95–GFP (black open squares, wild type; blue open squares, 1mΔ–2mΔ mutant; red open squares, 1mΔ–2mΔ–N326S mutant; filled squares, their averages). Insets are the plots of each cluster observed in one representative neuron. In the main graphs, each small square with bars indicates the averaged value ± SEM of each neuron [GFP intensity to the *x*-axis (arbitrary units) and IF intensity to the *y*-axis (arbitrary units)]. All of the cells analyzed expressed approximately similar amounts of PSD-95–GFP in the dendritic shaft, regardless of the mutant type. Therefore, the PSD-95–GFP intensities reflect the SCI values. ***B***, The IF intensities of a major PSD-95 ligand, synGAP, are significantly lower in the 1mΔ–2mΔ–N326S clusters (***B1***, red) and the 1mΔ–2mΔ clusters (***B2***, blue) compared with the PSD-95(WT)–GFP clusters (black). ***C–E***, In contrast, using the same assay, the IF intensities for other scaffold proteins distinct from PSD-95, such as Homer-1c (***C***), Shank/Synamon (***D***), and PSD-93/Chapsin-110 (***E***), are not significantly altered in the postsynaptic clusters ($p > 0.5$). *$p < 0.05$ versus WT by Student's t test.

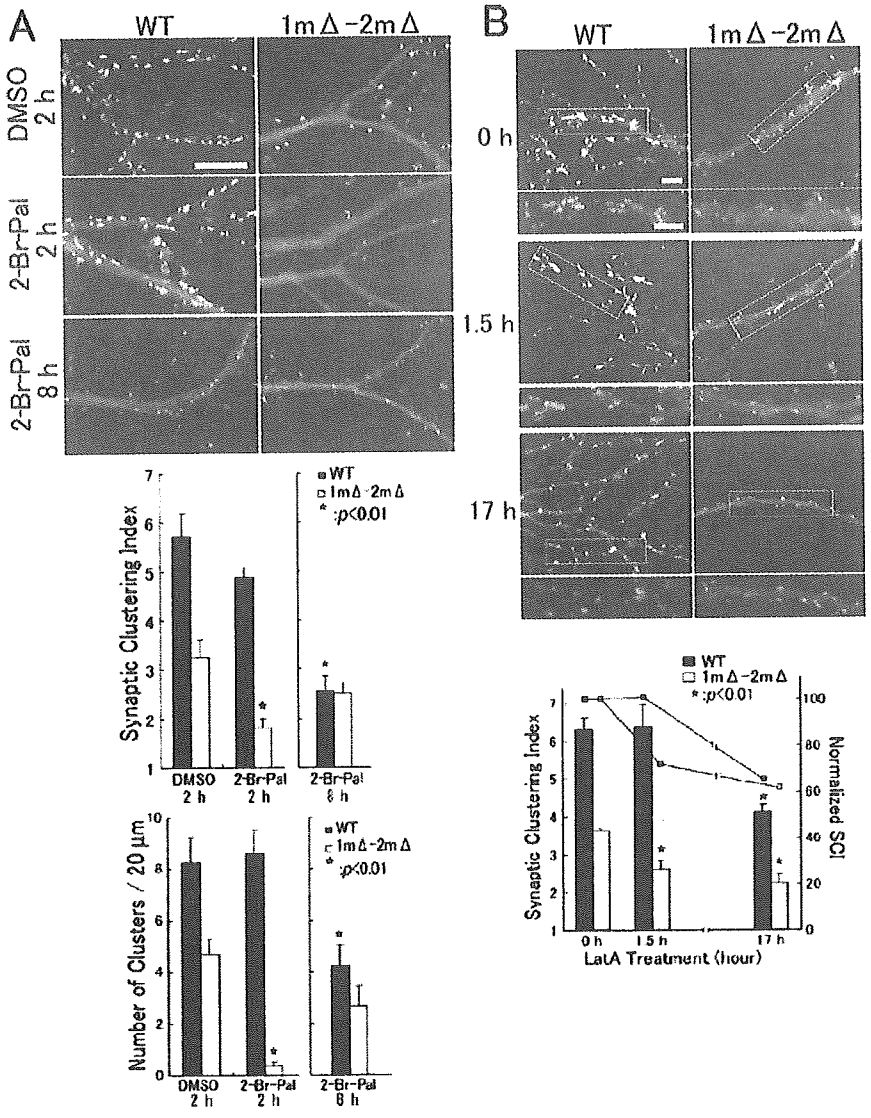

Figure 6. Ligand-binding-deficient mutants are more loosely anchored to the postsynaptic membrane than the wild type. *A*, Synaptic clusters in neurons expressing ligand-binding-deficient PSD-95 mutants are rapidly dispersed in response to treatment with a palmitoylation blocker, 2-Br-Pal. 2-Br-Pal dramatically reduces the clustering efficiencies in neurons expressing the mutant PSD-95 (1mΔ–2mΔ–N326S) but only moderately in neurons expressing the wild-type PSD-95. Grayscale images show the PSD-95–GFP fluorescence of the wild-type and 1mΔ–2mΔ-expressing neurons treated with DMSO or 2-Br-Pal for 2 or 8 h. The top graph summarizes the results of the SCI analysis of the DMSO-treated or 100 μM 2-Br-Pal-treated wild-type and 1mΔ–2mΔ-expressing neurons. The bottom graph shows the cluster density (number of clusters per 20 μm dendritic segment) of the same datasets. $*p < 0.01$ versus the SCI of DMSO 2 h by the Student's *t* test. *B*, Increased susceptibility to an actin-depolymerizing drug (LatA) in neurons expressing a ligand-binding-deficient mutant. Actin depolymerization by 5 μM latrunculin A caused much faster cluster dissociation in the 1mΔ–2mΔ mutant PSD-95-expressing neurons. Grayscale images of the wild-type and 1mΔ–2mΔ-expressing neurons treated with LatA for 0, 1.5, and 17 h. The small images below are the colored images (PSD-95–GFP, green) merged with synaptophysin staining (red) of the areas outlined by the white rectangles in the grayscale images. The graph shows the SCI values of the LatA-treated and nontreated wild-type and 1mΔ–2mΔ-expressing neurons. Raw values are shown as bar graphs (left *y*-axis), and scaled values (normalized to SCI at 0 h) are shown as line graphs (right *y*-axis). $*p < 0.01$ versus the SCI of nontreated (0 h) WT and 1mΔ–2mΔ, respectively, by the Student's *t* test. Scale bars, 10 μm.

previous experiments using 2-bromo-palmitate treatments, the mutant (1mΔ–2mΔ) PSD-95, during actin depolymerization, seemed to be more likely than the wild type to move away from synaptic clusters, although the presynaptic marker staining remained intact. Thus, the PDZ1/2 binding activity probably plays a critical role in facilitating postsynaptic clustering, in conjunction with a postsynaptic actin polymerization-dependent process.

Together, these data demonstrated that the clusters containing PDZ-binding-deficient PSD-95 mutants were more sensitive to treatment with a palmitoylation inhibitor or an actin depolymerization reagent. These results are consistent with the idea that efficient PDZ-ligand binding strongly promotes the clustering of PSD-95 and stabilizes the membrane anchoring, subsequent to a step after the activity-dependent palmitate cycling and the actin cytoskeleton-dependent attachment of the PSD-95 to the PSD complex.

These experiments alone may not formally rule out the possibility that the apparently increased susceptibility of the 1mΔ–2mΔ mutant-containing clusters to disperse during various manipulations (treatments with either a palmitoylation inhibitor or an actin depolymerization reagent) might be at least partially elicited by subtle reductions in the absolute amounts of expressed proteins in various local dendritic compartments rather than by a decrease in PDZ-ligand binding. We do not favor this interpretation, however, because the low expression level of wild-type PSD-95–GFP (less than the cutoff threshold of 100; see Materials and Methods) was not accompanied by a reduction in the SCI (data not shown).

To obtain independent support for the PDZ-ligand-binding-mediated stabilization of the localization of PSD-95 to the PSD, we performed additional quantitative measurements of PSD alterations, including spine morphology.

The PDZ-ligand-binding deficiency is correlated with a severe defect in the dendritic localization of PSD-95 clusters and may affect spine morphology

Consistent with the suggestion that the stability of PSD-95 may be compromised at postsynaptic clusters expressing PDZ-ligand-binding mutants, the overexpression of PSD-95–GFP with dysfunctional PDZ domains generated a significantly large number of synaptic clusters that were located away from the parent dendritic shaft (Figs. 3*D*,*H*,*J*, insets, 7*A*, 8) ($p < 0.001$, Kolmogorov–Smirnov test). In contrast, the wild-type PSD-95 clusters were formed directly on the dendritic shaft (Figs. 3*A*, 7*A*, 8), consistent with previous reports. To quantify this phenotype, we reanalyzed the same dataset of cells shown in Figures 3 and 4, measured the projected distance between each synaptic cluster and the closest dendritic shaft (cluster-shaft distance; when clusters were formed within the boundary of the dendritic shaft in a maximal projection image, the distance was considered as zero), and compared this index among the various types of mutants (Fig. 7*A*).

Most of the wild-type PSD-95 clusters were formed directly on

the dendrite (80.7% of the clusters were shaft clusters), and the average ± SEM apparent distance was 0.18 ± 0.029 μm, within the limit of the optical spatial resolution. Untransfected neurons analyzed with the anti-PSD-95 antibody staining produced a qualitatively similar value (0.10 ± 0.030 μm vs WT; $p > 0.05$, Kolmogorov–Smirnov test; data not shown), again within the limit of spatial resolution. In contrast, the average cluster-shaft distance of 1mΔ–2mΔ was significantly increased, to 0.47 ± 0.093 μm. In these 1mΔ–2mΔ expressing neurons, the cluster-shaft distance values showed a non-Gaussian distribution, which was quite distinct from that of the wild-type expressing neurons ($p < 0.001$, Kolmogorov–Smirnov test), with >40% of the clusters being significantly distant (this distance ranged from 0.2 to 3 μm) from the nearest shaft (Figs. 7*A*, 8). The clusters that formed far from dendrites did not form on immature filopodia/spines, because they were all juxtaposed with presynaptic markers, such as synaptophysin and VGLUT1 (Fig. 2). Thus, the formation and attraction of presynaptic boutons to the sites of PSD-95 clusters were not impaired at all, even in the PSD-95 mutant expressing neurons.

We wondered whether the PDZ-ligand-binding affinity might regulate this distance between the PSD-95 cluster and the shaft. To examine this possibility, we measured the cluster-shaft distance in all of the available PSD-95 mutants. Single PDZ mutants (1mΔ–2 or 1–2mΔ) had fewer shaft clusters (69.3 and 73.2%, respectively) compared with the wild type, and, in these cells, many clusters were found on the heads of spine-like protrusions. Similarly, in the PDZ3 N326S mutant expressing neurons, some of the clusters were formed on the spines, whereas 70.7% of the clusters were on the shafts (Fig. 8). The severest phenotype was found in the 1mΔ–2mΔ–N326S mutant expressing neurons, which had only 43.8% of the shaft clusters. Some of these were farther from the dendritic shafts and seemed to form on the cross-sections of thin, long protrusions from the dendrites.

Together, these data indicated that the average cluster-shaft distance was qualitatively (Fig. 3) and quantitatively (Figs. 7*A*, 8) longer in the mutant type with a lower SCI value. In fact, a statistically significant negative correlation was found between the SCI and the cluster-shaft distance (the coefficient of correlation, $r = -0.8637$; $p < 0.01$) (Fig. 7*B*).

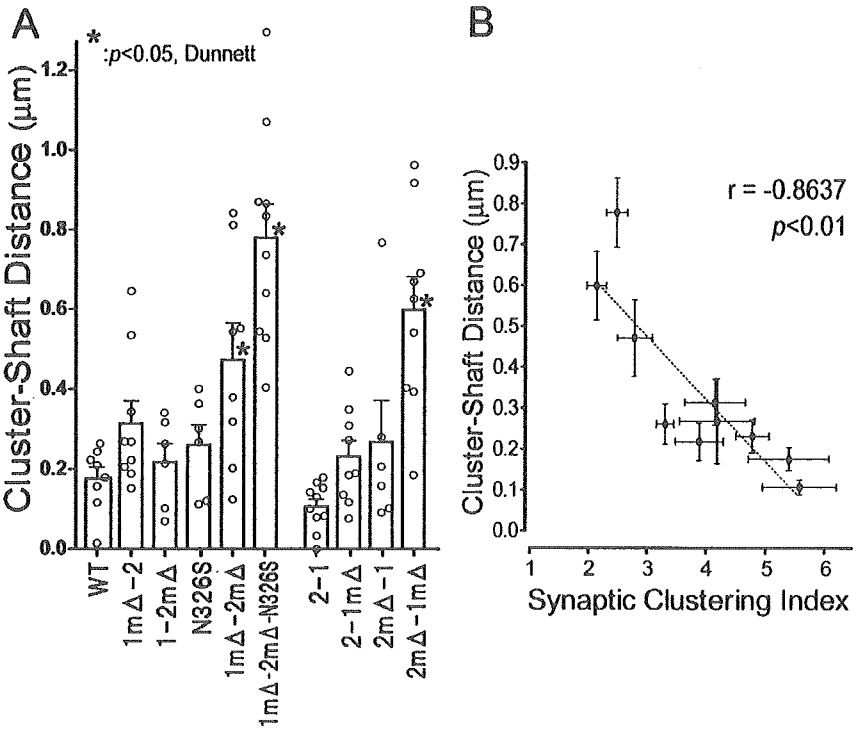

Figure 7. The cluster-shaft distance is increased in the mutant-expressing neurons compared with the wild-type-expressing neurons and negatively correlates with the SCI value. ***A***, Ligand-binding-deficient PSD-95 mutants formed clusters on tips of protrusions (spines) away from the dendritic shafts. The distance from the center of the synaptic clusters to the edge of the parent dendritic shaft was measured on the same dataset of cells used to calculate the SCI (Figs. 3, 4). To the shaft clusters (clusters that appeared to be formed directly on the dendritic shaft), the value 0 was arbitrarily assigned. Bars and error bars represent the averages and the SEMs of the calculated means of each cell (open dots). The error bars of WT and 2–1 are exceptionally small, because these cells predominantly have shaft clusters to which we applied the same values equally, and the large fraction of the shaft clusters will result in average distances below 0.2 μm. *$p < 0.05$ versus WT. ***B***, The SCI is negatively correlated with the cluster-shaft distance. The average SCI and the average cluster-shaft distance, the distance from the PSD-95 clusters to the dendritic shaft, of the wild type and each mutant type ($n = 6–10$ cells per mutant type), are plotted on the *x*-axis and *y*-axis, respectively. Error bars indicate SEM. The broken line shows the fitted regression line ($r = -0.8637$; $p < 0.01$).

The loss of PDZ binding in synGAP replicates the clustering and morphological phenotypes of PDZ-ligand-binding-deficient PSD-95

One candidate PDZ ligand that may be involved in the phenotypes associated with the overexpression of mutant PSD-95 is synGAP (Fig. 5). To directly test whether synGAP binding to PSD-95 is required for the efficient PSD-95 clustering and mature spine formation, we next examined the effects of overexpressing a synGAP C-terminal deletion mutant with diminished binding ability to the PDZ domains [synGAP(ΔSXV)]. We cotransfected the wild-type synGAP(TRV) with the intact C-terminal PDZ-binding motif or the mutant synGAP(ΔSXV), which lacks five C-terminal residues, QQTRV (Vazquez et al., 2004), together with the wild-type PSD-95–GFP. The expression of the synGAP(ΔSXV) caused the PSD-95(WT)–GFP to become distributed in an aberrant pattern with a reduced SCI, very similar to that of the ligand-binding-deficient PSD-95, i.e., 1mΔ–2mΔ (Fig. 9*A*,*B*). The localization of synGAP(ΔSXV) no longer overlapped with that of PSD-95, although many nonsynaptic synGAP clusters were detectable (Fig. 9*A*), presumably because of interactions with proteins other than PSD-95 (Tomoda et al., 2004). In contrast, the expression of the wild-type synGAP(TRV) did not change the pattern of PSD-95 localization, and the synGAP(TRV) colocalized well with the PSD-95 clusters (Fig. 9*A*,*B*). Similarly, the defect in synaptic clustering and the increase in cluster-shaft distance found in neurons expressing the 1mΔ–2mΔ mutant (Figs. 4, 7) were primarily replicated by the coexpression of PSD-95(WT)–GFP with the synGAP(ΔSXV) mutant (Fig. 9*C*,*D*). Consistently, the cluster density (the number of clusters per 20 μm dendritic segment) was greatly reduced in parallel (Fig. 9*C*), and, conversely, the cluster-shaft distance was elongated (Fig. 9*D*). This effect was specific for the PDZ-binding motif mutant synGAP(ΔSXV) and was not found with a mutant

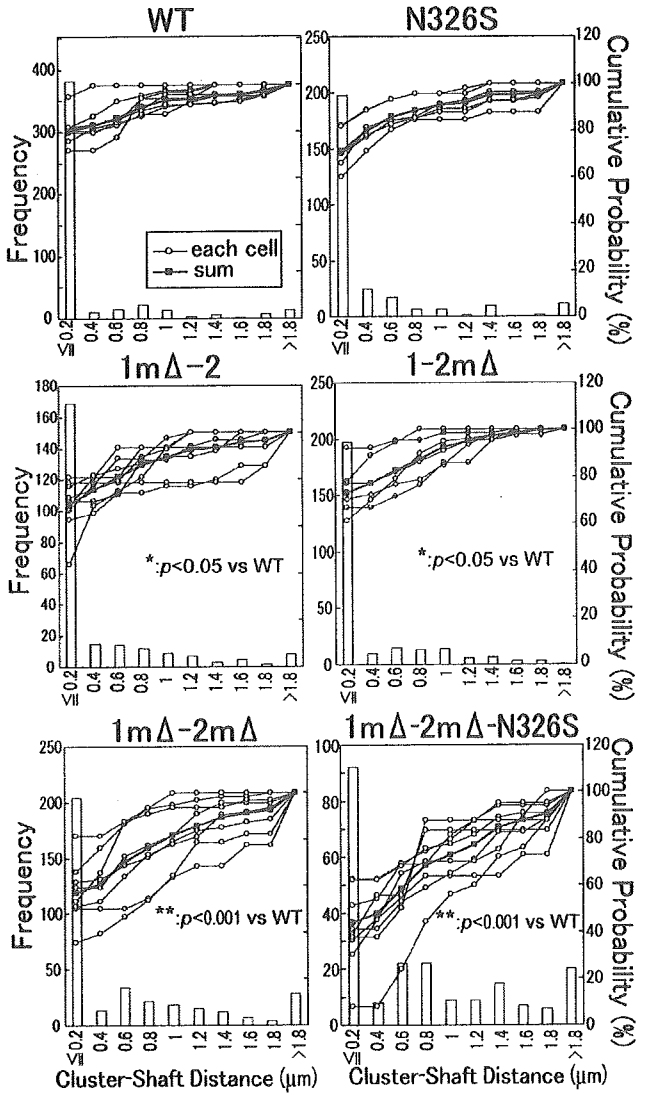

Figure 8. Histograms of the cluster-shaft distance distributions in the PSD-95 wild-type- and mutant-expressing neurons. The cumulative probability (right *y*-axis) of the cluster distances for each individual cell is traced (lines with open circles), and the aggregate data are traced (thicker lines with filled squares). The frequency histogram of the aggregate data were superimposed (left *y*-axis). Note that, in the mutant-expressing neurons, the cluster-shaft distance distribution cannot be fitted with a single Gaussian distribution, because they have a substantial portion of nonshaft clusters. This discrepancy is statistically significant. $*p < 0.05$ and $**p < 0.001$ versus WT by Kolmogorov–Smirnov test.

synGAP lacking GAP activity synGAP(GAP*) (data not shown). These data are consistent with the notion that the interaction of synGAP with the PDZ domains of PSD-95 may be essential for the efficient cluster formation at a higher density along the dendrites and the proper localization of the PSD-95 clusters closer to the dendritic shafts.

Additionally, we noticed that the combined expression of the 1mΔ–2mΔ mutant of PSD-95 and the synGAP(ΔSXV) mutant enhanced the phenotypes (reduced SCI, diminished synaptic clusters, and larger cluster-shaft distances) compared with neurons coexpressing the PSD-95(WT)–GFP in the presence of the synGAP(ΔSXV) mutant (Fig. 9*B–D*). Thus, primary PDZ ligands of PSD-95 distinct from synGAP may also contribute to the synaptic clustering and morphological phenotypes associated with decreased PDZ binding.

These findings together raise the possibility that the PDZ-ligand binding of PSD-95, in part via synGAP, may play a direct role in the synaptic clustering of PSD-95, while also directing the localization of PSD-95 containing clusters toward the vicinity of the dendritic shafts, perhaps during the final step of spine maturation.

Discussion

The localization and function of many essential synaptic proteins are regulated by molecular interactions with PDZ-containing scaffolding proteins. However, the molecular mechanisms that regulate the clustering of such PSD scaffolds at synapses are not fully understood. In this report, PDZ-ligand-binding-deficient, full-length PSD-95 mutants were used to probe the contribution of each of the three PDZ-ligand-binding affinities in various aspects of PSD-95-mediated PSD organization.

Independent and additive contributions of each PDZ domain to PSD-95 clustering and recruiting PDZ ligands to the PSD scaffold

Previous studies showed that at least one PDZ domain was needed to target the PSD-95 to the synapse, in addition to the requirement of the N-terminal region including the palmitoylated pair of cysteines, which is essential for multimerization and membrane targeting (Craven et al., 1999; Hsueh and Sheng, 1999; Christopherson et al., 2003). Furthermore, the inhibition of the PDZ3 binding to the microtubule-binding protein CRIPT impaired the synaptic clustering of the PSD-95 (Passafaro et al., 1999). We also found that overexpression of a ligand-binding-deficient PDZ3 mutant of PSD-95 with a single point mutation, in cultured hippocampal neurons, significantly reduced the clustering efficiency of PSD-95 at synapses. This indicated that the interaction between the PDZ3 and its ligand(s) plays an important role in clustering PSD-95 at the synapses. Importantly, by extending the mutagenesis to the ligand-binding sites of PDZ1 and PDZ2, we demonstrated that the ligand-binding activities of PDZ1 and PDZ2 were equally critical for the efficient clustering of PSD-95. Furthermore, the impact of losing the PDZ-binding affinities one by one accumulated in an approximately additive manner. Thus, our data indicated that each individual binding event at each PDZ domain of PSD-95 independently and approximately additively contributes to the additional clustering of PSD-95 at the synapses.

We further verified this conclusion by a mutant study using one of the major ligand proteins, synGAP. The absence of the PDZ-binding motif of synGAP produced a pattern of results quite similar to those obtained with the ligand-binding-deficient PSD-95 mutants and strongly affected both the PSD-95 clustering and the spine morphology. In keeping with the results obtained by a systematic introduction of the mutations to the PDZ domains, the synGAP mutant data suggested that the presence of PSD-95 ligand-binding motifs is not sufficient, but rather an intact synGAP-PSD-95 interaction, mediated via PDZ-binding, is necessary for the clustering and the functions of PSD-95.

Our results also revealed that the ligand-binding-deficient mutants exhibited significantly weaker associations with the PSD. The 2-bromo-palmitate treatment easily dispersed the mutant PSD-95–GFP molecules from their clusters. These results support the notion that PSD-95 is anchored to the PSD by both the palmitate modification and the ligand-PDZ domain interactions. Furthermore, the clusters expressing PSD-95 mutants became extremely labile after F-actin depolymerization by the LatA treatment, consistent with the possibility that the mutant PSD-95

was unable to reach the core fraction of the PSD and thus became mislocalized toward the peripheral, cytoskeleton-dependent fraction of the PSD (Allison et al., 2000; Zhang and Benson, 2001). Together, the data suggested that the tight and stable association of PSD-95 with the PSD requires the interactions of the PDZ domains with their ligands, as well as the appropriate PSD-95 lipidification and actin polymerization.

Our results also suggested that each ligand-binding event at the PDZ domains may additionally fulfill two other separate functions in parallel: efficient targeting of PSD-95 to the spines, and stable recruitment and incorporation of PSD-95 ligands into the PSD. In this regard, it may be useful to consider two distinct classes of PSD-95 ligands: one class including PSD-95-specific ligands, such as synGAP, and another class that includes scaffold-independent ligands, such as NMDA receptor subunits, which, for example, can tightly interact with synapse-associated protein 102 (SAP102) as well. Although the latter may still become localized to the synapses in the absence of PSD-95 (Migaud et al., 1998; Rao et al., 1998), our data suggested that PDZ-ligand binding strongly contributes to the tight association of these two classes of proteins as stable multiprotein networks in the vicinity of synapses.

Another implication of our work, in view of the approximately additive effect of the three PDZ domains in the clustering of PSD-95, is that the tightness of the PSD association with the PSD protein complex may be tuned and controlled as a function of the number of PDZ-ligand-binding events. The intermolecular MAGUK interaction is reportedly activity regulated, at least in the case of SAP97 (Nakagawa et al., 2004). Whether this activity dependence in MAGUK clustering and dispersion is actually mediated by the PDZ-ligand binding still remains to be demonstrated. If this is the case, then the clustering efficiency of the MAGUK-like scaffolds, such as PSD-95, could be dynamically modulated depending on the local synaptic activity, thereby accounting for the requirement for multivalent scaffolding proteins in the regulation of synaptic plasticity (Migaud et al., 1998; Ehrlich and Malinow, 2004; Nakagawa et al., 2004).

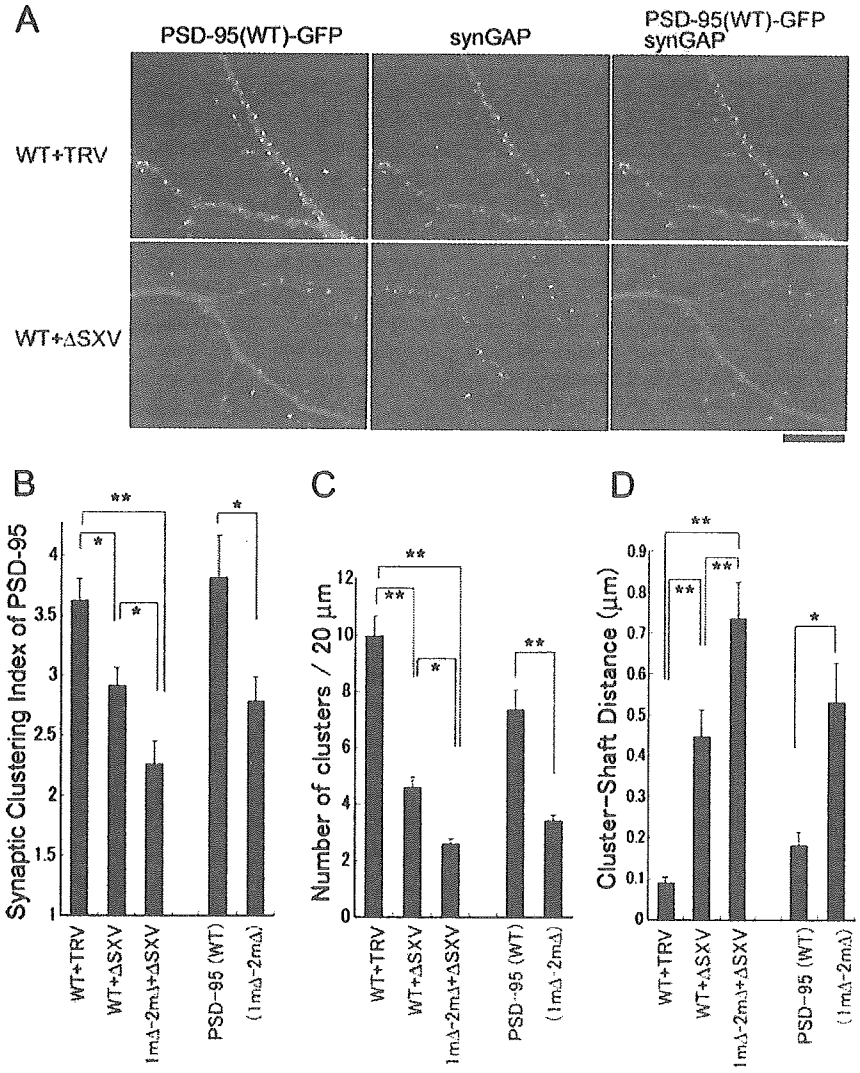

Figure 9. Overexpression of a mutant synGAP lacking the C-terminal PDZ-binding motif results in a severe defect in the PSD-95 cluster formation and a significant increase in the PSD-95 cluster-shaft distance. ***A***, Immunolocalization of PSD-95 clusters [PSD-95(WT)–GFP] and synGAP in neurons coexpressing the wild-type PSD-95 and either the wild-type synGAP (TRV, top panels) or the PDZ-binding motif mutant synGAP (ΔSXV, bottom panels). Neurons were cotransfected at 8 DIV and fixed at 10 DIV. The coexpression of wild-type synGAP(TRV) with wild-type PSD-95 did not result in a detectable change in the clustering efficiency and cluster density compared with the overexpression of PSD-95(WT)–GFP alone. Remarkably, during coexpression with synGAP(ΔSXV), PSD-95(WT)–GFP displayed an aberrant dendritic distribution that was similar to the phenotypes seen with the ligand-binding-deficient PSD-95 mutant (i.e., 1mΔ–2mΔ). ***B–D***, Quantification of the defects seen in synaptic cluster formation and in spine morphology. Based on the images of PSD-95–GFP, the SCI values (***B***), the cluster density (the number of synaptic clusters per 20 μm dendritic segment) (***C***), and the cluster-shaft distance (***D***) were measured in the neurons expressing the indicated constructs and are shown as bar graphs. We confirmed that the PSD-95 clusters analyzed were all juxtaposed to the synaptophysin-staining puncta. Scale bar, 10 μm. $*p < 0.05$, $**p < 0.01$, by one-way ANOVA with *post hoc* Tukey's test (n = 12–16 neurons); or $*p < 0.05$, $**p < 0.01$, by the Student's t test in the experimental pairs of PSD-95(WT)–GFP only and PSD-95(1mΔ–2mΔ)–GFP only.

Possible recruitment of a morphogenic signaling complex via PSD-95 during synapse development

In our hands, the ligand-binding-deficient PSD-95 not only reduced the clustering efficiency and altered the composition of the PSD but also localized its own clusters far from the dendritic shafts in hippocampal neurons (Figs. 3, 7). The aberrant PSD cluster location and the higher frequency of elongated spine morphology were consistently observed in both a transient plasmid expression protocol by gene delivery at 8–9 DIV and after a long-term expression protocol by electroporation at 0 DIV, with subsequent 12–13 d cultures. Because no gross morphological change was reported in the PSD-95 knock-out mouse (Migaud et al., 1998), it may appear, at first glance, that the defect in the PSD cluster localization seen in our culture could be interpreted as an experimental artifact. However, we believe that this is not the case for two reasons. First, the PSD location and the spine morphol-

ogy defects are not observed in all spines but only in a minority of the spines within a mutant PSD-95 expressing neuron (at most, 20.8% of spines longer than 1 μm, even in the severest case). Therefore, a large-scale quantification study in the knock-out mice brain, using serial electron microscopy over entire dendritic trees, would be needed to corroborate our findings, but such an effort was not undertaken in the initial screen (Migaud et al., 1998). Second, we observed correlations not only between the synaptic clustering index and the cluster-shaft distance (a negative correlation) but also between the PSD-95 cluster formation and the synGAP recruitment (a positive correlation). Indeed, synGAP, a GTPase-activating protein for Ras, was less densely localized at postsynaptic sites in the 1mΔ–2mΔ–N326S expressing neurons, whereas Shank/Synamon, Homer 1c/Ves1-L/PSD-Zip45, and PSD-93/Chapsin-110 were normally localized, as in the wild-type PSD-95 expressing neurons. Most critically, a synGAP mutant lacking the C-terminal PDZ-binding motif showed effects similar to those seen with PSD-95 mutants. These results are consistent with the idea that synGAP, in part downstream of PSD-95, may function in the clustering and movement of the PSD proteins in the spines. Furthermore, synGAP reportedly also negatively regulates spine formation and limits spine head expansion and filopodial extension (Vazquez et al., 2004). Together, alterations in the distribution and the PSD clustering of synGAP may at least partially account for the aberrant phenotype observed in cultured neurons. Thus, PSD-95 may play a role in recruiting a morphogenic signaling complex within the PSD complex.

Such a view is consistent with the following experimental results. (1) The morphological changes associated with the wild-type PSD-95 overexpression were shown to increase both the number and size of the spines, together with the accelerated synaptic maturation (El-Husseini et al., 2000). (2) Several partners interacting with PSD-95, such as Citron (Furuyashiki et al., 1999), CRIPT (Niethammer et al., 1998), and SPAR (spine-associated RapGAP) (Pak et al., 2001), were shown to interact with cytoskeletal elements. The overexpression of related scaffold proteins, such as Homer and Shank, which closely interact with actin cytoskeletal components (Naisbitt et al., 1999; Shiraishi et al., 1999), reportedly induces spine head enlargement (Sala et al., 2001). (3) A growing list of morphogenic signaling molecules has been identified within the PSD complex, such as FMR1 (the fragile X mental retardation gene) (Comery et al., 1997; Nimchinsky et al., 2001), LIM kinase (Meng et al., 2002), N-cadherin (Togashi et al., 2002), ephrinA3-EphA4 (Murai et al., 2003), cortactin (Hering and Sheng, 2003), Rho-GEF (guanine nucleotide exchange factor) Kalirin-7 (Penzes et al., 2001), and EphB2 (Murai et al., 2003). Because PSD-95-ligand binding is critical for maintaining proper PSD organization, impairments of the scaffolding functions of PSD-95 might indirectly disrupt the PSD localization and the spine maturation by triggering the misorchestration of a morphogenic signaling complex.

In summary, this work demonstrates that the ligand-binding activities of each of the three PDZ domains are essential for PSD-95 to organize the PSD properly and are likely to be involved in achieving normal spine development, in part via interactions with synGAP. We found that the multivalent binding nature of PSD-95 plays a key role in the dynamic regulation of PSD protein clustering. Our study thus provides new insights into the structural basis of the role of PSD-95 in synaptic development and plasticity.

References

Allison DW, Gelfand VI, Spector I, Craig AM (1998) Role of actin in anchoring postsynaptic receptors in cultured hippocampal neurons: differential attachment of NMDA versus AMPA receptors. J Neurosci 18:2423–2436.

Allison DW, Chervin AS, Gelfand VI, Craig AM (2000) Postsynaptic scaffolds of excitatory and inhibitory synapses in hippocampal neurons: maintenance of core components independent of actin filaments and microtubules. J Neurosci 20:4545–4554.

Arnold DB, Clapham DE (1999) Molecular determinants for subcellular localization of PSD-95 with an interacting K^+ channel. Neuron 23:149–157.

Brenman JE, Topinka JR, Cooper EC, McGee AW, Rosen J, Milroy T, Ralston HJ, Bredt DS (1998) Localization of postsynaptic density-93 to dendritic microtubules and interaction with microtubule-associated protein 1A. J Neurosci 18:8805–8813.

Chen HJ, Rojas-Soto M, Oguni A, Kennedy MB (1998) A synaptic Ras-GTPase activating protein (p135 SynGAP) inhibited by CaM kinase II. Neuron 20:895–904.

Cho KO, Hunt CA, Kennedy MB (1992) The rat brain postsynaptic density fraction contains a homolog of the *Drosophila* discs-large tumor suppressor protein. Neuron 9:929–942.

Christopherson KS, Sweeney NT, Craven SE, Kang R, El-Husseini Ael D, Bredt DS (2003) Lipid- and protein-mediated multimerization of PSD-95: implications for receptor clustering and assembly of synaptic protein networks. J Cell Sci 116:3213–3219.

Comery TA, Harris JB, Willems PJ, Oostra BA, Irwin SA, Weiler IJ, Greenough WT (1997) Abnormal dendritic spines in fragile X knockout mice: maturation and pruning deficits. Proc Natl Acad Sci USA 94:5401–5404.

Craven SE, El-Husseini AE, Bredt DS (1999) Synaptic targeting of the postsynaptic density protein PSD-95 mediated by lipid and protein motifs. Neuron 22:497–509.

Ehrlich I, Malinow R (2004) Postsynaptic density 95 controls AMPA receptor incorporation during long-term potentiation and experience-driven synaptic plasticity. J Neurosci 24:916–927.

El-Husseini AE, Schnell E, Chetkovich DM, Nicoll RA, Bredt DS (2000) PSD-95 involvement in maturation of excitatory synapses. Science 290:1364–1368.

El-Husseini Ael D, Schnell E, Dakoji S, Sweeney N, Zhou Q, Prange O, Gauthier-Campbell C, Aguilera-Moreno A, Nicoll RA, Bredt DS (2002) Synaptic strength regulated by palmitate cycling on PSD-95. Cell 108:849–863.

Furuyashiki T, Fujisawa K, Fujita A, Madaule P, Uchino S, Mishina M, Bito H, Narumiya S (1999) Citron, a Rho-target, interacts with PSD-95/SAP-90 at glutamatergic synapses in the thalamus. J Neurosci 19:109–118.

Furuyashiki T, Arakawa Y, Takemoto-Kimura S, Bito H, Narumiya S (2002) Multiple spatiotemporal modes of actin reorganization by NMDA receptors and voltage-gated Ca^{2+} channels. Proc Natl Acad Sci USA 99:14458–14463.

Hammer O, Harper DAT, Ryan PD (2001) PAST: paleontological statistics software package for education and data analysis. Palaeontologia Electronica 4:9.

Hering H, Sheng M (2003) Activity-dependent redistribution and essential role of cortactin in dendritic spine morphogenesis. J Neurosci 23:11759–11769.

Hsueh YP, Sheng M (1999) Requirement of N-terminal cysteines of PSD-95 for PSD-95 multimerization and ternary complex formation, but not for binding to potassium channel Kv1.4. J Biol Chem 274:532–536.

Imamura F, Maeda S, Doi T, Fujiyoshi Y (2002) Ligand binding of the second PDZ domain regulates clustering of PSD-95 with the Kv1.4 potassium channel. J Biol Chem 277:3640–3646.

Irie K, Nakatsu T, Mitsuoka K, Miyazawa A, Sobue K, Hiroaki Y, Doi T, Fujiyoshi Y, Kato H (2002) Crystal structure of the Homer 1 family conserved region reveals the interaction between the EVH1 domain and own proline-rich motif. J Mol Biol 318:1117–1126.

Irie M, Hata Y, Takeuchi M, Ichtchenko K, Toyoda A, Hirao K, Takai Y, Rosahl TW, Sudhof TC (1997) Binding of neuroligins to PSD-95. Science 277:1511–1515.

Kim E, Niethammer M, Rothschild A, Jan YN, Sheng M (1995) Clustering of Shaker-type K^+ channels by interaction with a family of membrane-associated guanylate kinases. Nature 378:85–88.

Kim JH, Liao D, Lau LF, Huganir RL (1998) SynGAP: a synaptic RasGAP that associates with the PSD-95/SAP90 protein family. Neuron 20:683–691.

Kornau HC, Schenker LT, Kennedy MB, Seeburg PH (1995) Domain interaction between NMDA receptor subunits and the postsynaptic density protein PSD-95. Science 269:1737–1740.

Long JF, Tochio H, Wang P, Fan JS, Sala C, Niethammer M, Sheng M, Zhang M (2003) Supramodular structure and synergistic target binding of the N-terminal tandem PDZ domains of PSD-95. J Mol Biol 327:203–214.

McGee AW, Dakoji SR, Olsen O, Bredt DS, Lim WA, Prehoda KE (2001) Structure of the SH3-guanylate kinase module from PSD-95 suggests a mechanism for regulated assembly of MAGUK scaffolding proteins. Mol Cell 8:1291–1301.

Meng Y, Zhang Y, Tregoubov V, Janus C, Cruz L, Jackson M, Lu WY, MacDonald JF, Wang JY, Falls DL, Jia Z (2002) Abnormal spine morphology and enhanced LTP in LIMK-1 knockout mice. Neuron 35:121–133.

Migaud M, Charlesworth P, Dempster M, Webster LC, Watabe AM, Makhinson M, He Y, Ramsay MF, Morris RG, Morrison JH, O'Dell TJ, Grant SG (1998) Enhanced long-term potentiation and impaired learning in mice with mutant postsynaptic density-95 protein. Nature 396:433–439.

Murai KK, Nguyen LN, Irie F, Yamaguchi Y, Pasquale EB (2003) Control of hippocampal dendritic spine morphology through ephrin-A3/EphA4 signaling. Nat Neurosci 6:153–160.

Naisbitt S, Kim E, Tu JC, Xiao B, Sala C, Valtschanoff J, Weinberg RJ, Worley PF, Sheng M (1999) Shank, a novel family of postsynaptic density proteins that binds to the NMDA receptor/PSD-95/GKAP complex and cortactin. Neuron 23:569–582.

Nakagawa T, Futai K, Lashuel HA, Lo I, Okamoto K, Walz T, Hayashi Y, Sheng M (2004) Quaternary structure, protein dynamics, and synaptic function of SAP97 controlled by L27 domain interactions. Neuron 44:453–467.

Niethammer M, Valtschanoff JG, Kapoor TM, Allison DW, Weinberg TM, Craig AM, Sheng M (1998) CRIPT, a novel postsynaptic protein that binds to the third PDZ domain of PSD-95/SAP90. Neuron 20:693–707.

Nimchinsky EA, Oberlander AM, Svoboda K (2001) Abnormal development of dendritic spines in FMR1 knock-out mice. J Neurosci 21:5139–5146.

Okabe S, Kim HD, Miwa A, Kuriu T, Okado H (1999) Continual remodeling of postsynaptic density and its regulation by synaptic activity. Nat Neurosci 2:804–811.

Pak DT, Yang S, Rudolph-Correia S, Kim E, Sheng M (2001) Regulation of dendritic spine morphology by SPAR, a PSD-95-associated RapGAP. Neuron 31:289–303.

Passafaro M, Sala C, Niethammer M, Sheng M (1999) Microtubule binding by CRIPT and its potential role in the synaptic clustering of PSD-95. Nat Neurosci 2:1063–1069.

Penzes P, Johnson RC, Sattler R, Zhang X, Huganir RL, Kambampati V, Mains RE, Eipper BA (2001) The neuronal Rho-GEF Kalirin-7 interacts with PDZ domain-containing proteins and regulates dendritic morphogenesis. Neuron 29:229–242.

Petersen JD, Chen X, Vinade L, Dosemeci A, Lisman JE, Reese TS (2003) Distribution of postsynaptic density (PSD)-95 and Ca^{2+}/calmodulin-dependent protein kinase II at the PSD. J Neurosci 23:11270–11278.

Rao A, Kim E, Sheng M, Craig AM (1998) Heterogeneity in the molecular composition of excitatory postsynaptic sites during development of hippocampal neurons in culture. J Neurosci 18:1217–1229.

Sala C, Piech V, Wilson NR, Passafaro M, Liu G, Sheng M (2001) Regulation of dendritic spine morphology and synaptic function by Shank and Homer. Neuron 31:115–130.

Sheng M, Sala C (2001) PDZ domains and the organization of supramolecular complexes. Annu Rev Neurosci 24:1–29.

Shiraishi Y, Mizutani A, Bito H, Fujisawa K, Narumiya S, Mikoshiba K, Furuichi T (1999) Cupidin, an isoform of Homer/Vesl, interacts with the actin cytoskeleton and activated rho family small GTPases and is expressed in developing mouse cerebellar granule cells. J Neurosci 19:8389–8400.

Sprengel R, Single FN (1999) Mice with genetically modified NMDA and AMPA receptors. Ann NY Acad Sci 868:494–501.

Takemoto-Kimura S, Terai H, Takamoto M, Ohmae S, Kikumura S, Segi E, Arakawa Y, Furuyashiki T, Narumiya S, Bito H (2003) Molecular cloning and characterization of CLICK-III/CaMKIgamma, a novel membrane-anchored neuronal Ca^{2+}/calmodulin-dependent protein kinase (CaMK). J Biol Chem 278:18597–18605.

Tavares GA, Panepucci EH, Brunger AT (2001) Structural characterization of the intramolecular interaction between the SH3 and guanylate kinase domains of PSD-95. Mol Cell 8:1313–1325.

Togashi H, Abe K, Mizoguchi A, Takaoka K, Chisaka O, Takeichi M (2002) Cadherin regulates dendritic spine morphogenesis. Neuron 35:77–89.

Tomoda T, Kim JH, Zhan C, Hatten ME (2004) Role of Unc51.1 and its binding partners in CNS axon outgrowth. Genes Dev 18:541–558.

Vazquez LE, Chen HJ, Sokolova I, Knuesel I, Kennedy MB (2004) SynGAP regulates spine formation. J Neurosci 24:8862–8872.

Zhang W, Benson DL (2001) Stages of synapse development defined by dependence on F-actin. J Neurosci 21:5169–5181.

Pax6 is required for production and maintenance of progenitor cells in postnatal hippocampal neurogenesis

Motoko Maekawa[1,3], Noriko Takashima[1,2], Yoko Arai[1], Tadashi Nomura[1], Kaoru Inokuchi[2], Shigeki Yuasa[3] and Noriko Osumi[1,4,*]

[1]*Division of Developmental Neuroscience, Center for Translational and Advanced Animal Research (CTAAR), Tohoku University School of Medicine, 2-1 Seiryo-machi, Aoba-ku, Sendai 980-8575, Japan*

[2]*Mitsubishi Kagaku Institute of Life Sciences (MITILS), Minamiooya 11, Machida, Tokyo 194-8511, Japan*

[3]*Department of Ultrastructural Research, National Institute of Neuroscience, National Center of Neurology and Psychiatry, 4-1-1 Ogawahigashi-machi, Kodaira, Tokyo 187-8502, Japan*

[4]*CREST, Japan Science and Technology Corporation (JST), 4-1-8 Honmachi, Kawaguchi, 332-0012, Japan*

Neurogenesis is crucial for brain formation and continues to take place in certain regions of the postnatal brain including the subgranular zone (SGZ) of the hippocampal dentate gyrus (DG). Pax6 transcription factor is a key player for patterning the brain and promoting embryonic neurogenesis, and is also expressed in the SGZ. In the DG of wild-type rats, more than 90% of total BrdU-incorporated cells expressed Pax6 at 30 min time point after BrdU injection. Moreover, approximately 60% of Pax6$^+$ cells in the SGZ exhibited as GFAP$^+$ cells with a radial glial phenotype and about 30% of Pax6$^+$ cells exhibited as PSA-NCAM$^+$ cells in clusters. From BrdU labeling for 3 days, we found that cell proliferation was 30% decreased at postnatal stages in *Pax6*-deficient *rSey*^{2}/+ rat. BrdU pulse/chase experiments combined with marker staining revealed that PSA-NCAM$^+$ late progenitor cells increased at the expense of GFAP$^+$ early progenitors in *rSey*^{2}/+ rat. Furthermore, expression of Wnt ligands in the SGZ was markedly reduced in *rSey*^{2}/+ rat. Taken all together, an appropriate dosage of Pax6 is essential for production and maintenance of the GFAP$^+$ early progenitor cells in the postnatal hippocampal neurogenesis.

Introduction

Neurogenesis depends on a specific population of cells termed 'neural stem/progenitor cells' (we call here 'neural progenitor cells'). In the mammalian embryonic brain, neural progenitor cells take a feature of 'neuroepithelial cells' or 'matrix cells' (reviewed in Fujita 2003) while the adult brain contains islands of neural progenitor cells in the subventricular zone (SVZ) of the lateral ventricle and in the subgranular zone (SGZ) of the hippocampal dentate gyrus (DG) (Altman & Das 1965 and see reviews by Gage 2000; Alvarez-Buylla *et al.* 2002). These cells possess pluripotent differentiation potential; they can become neurons, astrocytes, or oligodendrocytes.

In hippocampal neurogenesis, dividing precursor cells give rise to daughter cells, which migrate away from the SGZ and start to differentiate into neurons (Seki & Arai 1993; Kuhn *et al.* 1996; Kempermann *et al.* 2003). Several lines of evidence have suggested that there are distinct subtypes of neural progenitor cells in the SGZ. In electron microscopy analysis, there are two types of mitotically active SGZ cells; type B cells that have ultrastructural features of astrocytes with light cytoplasm containing GFAP and multiple processes, rapidly convert into type D cells that are small electron-dense cells and GFAP negative (Seri *et al.* 2001). Another paper (Fukuda *et al.* 2003) has shown two distinct progenitor cells based on morphology, molecular expression, and electrical features: GFAP$^+$ type I cells with lower input resistance (IR) and PSA-NCAM$^+$ type II cells with higher IR. Roughly speaking, type I cells correspond to B cells, while type II cells to D cells. In this paper, we use GFAP$^+$ early progenitors and PSA-NCAM$^+$ late progenitors as clearer definition.

Although adult and embryonic neurogenesis differs in some aspects, there indeed is similarity. In the adult

Communicated by: Tetsuya Taga
**Correspondence*: E-mail: osumi@mail.tains.tohoku.ac.jp

DOI: 10.1111/j.1365-2443.2005.00893.x

hippocampus, GFAP$^+$ early progenitors have the appearance of radial glial cells, and not only do they produce neurons but also provide scaffolding for migration of newly born neurons (Forster *et al.* 2002). These features are quite similar to embryonic radial glial cells that constitute the ventricular zone (Gotz 2003; Tramontin *et al.* 2003). The finding that radial glia-like cells in the adult brain have stem cell properties (Doetsch *et al.* 1997, 1999; Seri *et al.* 2001) leads us to search for intrinsic molecular mechanisms that commonly govern pre- and postnatal neurogenesis.

A transcription factor Pax6 is strongly expressed during brain development in the discrete regions such as the dorsal telencephalon and the ventral hindbrain and serves as one of the key factor for patterning the central nervous system (see reviews by Osumi 2001; Simpson & Price 2002). Specific Pax6 expression is observed in the nucleus of the ventricular zone cells, which are most likely radial glial cells (Gotz 2003). In a spontaneous mutant *Small eye* (*Sey*) mouse that lacks functional Pax6, radial glial cells are less in number and show a distorted morphology, altered gene expression patterns and abnormal cell cycle characteristics (Stoykova *et al.* 1997; Gotz *et al.* 1998; Estivill-Torrus *et al.* 2002). A similar observation that less PCNA-positive cells constitute the thinner ventricular zone in *Small eye* rat mutant (*rSey*^{2}) has also been reported (Fukuda *et al.* 2000). Curiously enough, Pax6 is expressed not only in the embryonic neuroepithelium but also in the adult brain including the SGZ and the SVZ (Stoykova & Gruss 1994; Nakatomi *et al.* 2002; Hack *et al.* 2004, 2005); the above-mentioned regions which are known as the places that neurogenesis persists in adulthood. All these lines of evidences have prompted us to examine the role of Pax6 in postnatal neurogenesis.

Here, we show that Pax6-expressing cells in the SGZ of the hippocampus have a neural progenitor-like character at the molecular and the cellular levels. Detailed BrdU pulse/chase experiments have revealed that the ratio of GFAP$^+$ early progenitor cells in total BrdU$^+$ cells decreased, and instead, PSA-NCAM$^+$ late progenitors increased in the *Pax6*-deficient *rSey*^{2}/+ rat. Therefore Pax6 is necessary for the maintenance of the GFAP$^+$ early progenitor cells in the SGZ. We further searched for Pax6 downstream molecules that are relevant for the proliferation of neural progenitor cells in postnatal hippocampus, and found that expressions of Wnt ligands *Wnt7a* and *Wnt7b* and downstream effecter *Dvl1* are changed in the DG of the *rSey*^{2}/+. Our results suggest that a genetic cascade of Pax6–Wnt is critical for postnatal hippocampal neurogenesis especially at the early step.

Results

Pax6-positive cells express early progenitor markers

Previous studies have reported that Pax6 is expressed in discrete regions of the postnatal brain such as the cerebellum and the limbic system including the olfactory bulb, olfactory cortex, and hippocampus (Stoykova & Gruss 1994; Nakatomi *et al.* 2002; Hack *et al.* 2004). In the present study, we focused on Pax6 expression in the DG of which knowledge on adult neurogenesis has been gathered.

In the DG of the wild-type rat at 4 weeks when the architecture of the hippocampus is established, many Pax6$^+$ cells were observed in unique distribution patterns (Fig. 1A). A majority of Pax6$^+$ cells were located in the SGZ, sometimes in clusters of five to eight cells (Fig. 1A,C). A much smaller number of Pax6$^+$ cells were detectable in the hilus and molecular layer, whereas Pax6$^+$ cells were scarcely found in the granule cell layer (GCL). To elucidate the character of Pax6$^+$ cells, we performed double labeling with various markers for neural progenitor cells, neurons, and astrocytes (Fig. 1B,C). Many of Pax6$^+$ cells co-expressed GFAP, a marker for astrocytes or early progenitors marker (59.0%, 85/144 cells; Fig. 1B,C), and a majority of Pax6/GFAP double-positive cells had processes oriented radially into the GCL of the DG (Fig. 1C,C′; also see Fig. 5E). Pax6$^+$ cells also expressed neural stem cell markers nestin (34.4%, 20/58 cells) and Musashi1 (68.7%, 22/32 cells) (Fig. 1B). About a third of Pax6$^+$ cells co-expressed a late progenitor marker PSA-NCAM (31.5%, 41/130 cells) (Fig. 1B). Contrastingly, Pax6$^+$ cells scarcely expressed neuronal marker NeuN (1.9%: 12/652 cells) (Fig. 1B). These results suggest that Pax6$^+$ cells exhibited the neural progenitor cell-like character.

In immuno-electron microscopy, most of Pax6$^+$ cells had irregular contours and light cytoplasm containing a few ribosomes and glial filaments (Fig. 1D,D′), showing a character of B cell (Seri *et al.* 2001). A few Pax6$^+$ cells had smooth contours and dark scant cytoplasm negative for intermediate filaments (Fig. 1E,E′), showing a character of D cell (Seri *et al.* 2001). We sometimes observed Pax6$^+$ cells that had thinner and feeble glial filaments and scant dark cytoplasm, representing an intermediate character of B cell and D cell. These data suggest that more than half of Pax6$^+$ cells show morphologic features of the GFAP$^+$ early progenitor cells in the DG.

Defects in the DG of *rSey*^{2}/+ rats

In order to elucidate the role of Pax6 in hippocampal neurogenesis, we first observed the DG of *Pax6*-deficient

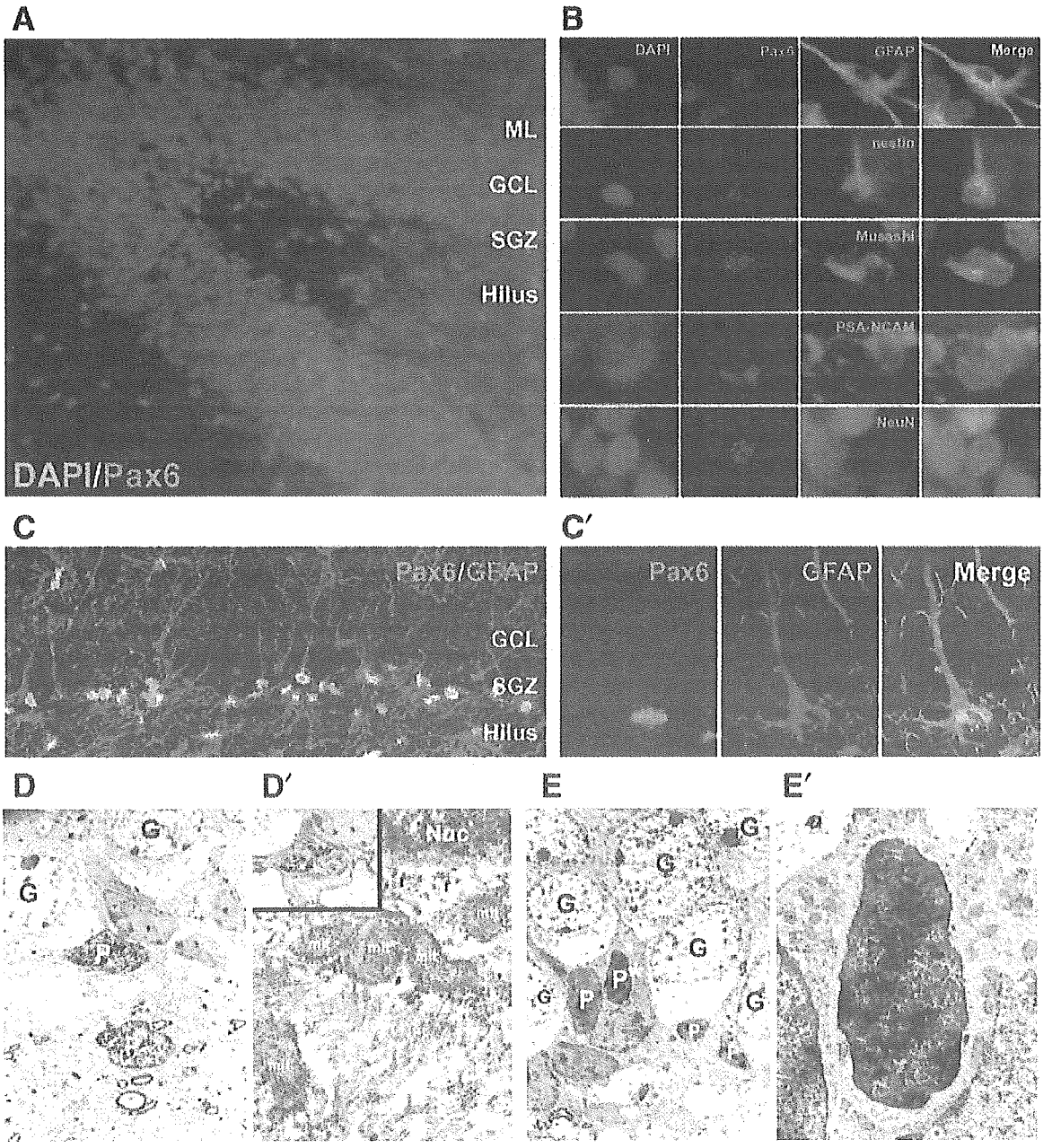

Figure 1 Pax6$^+$ cells in the DG of the 4-week-old wild-type rat. (A) Many Pax6$^+$ cells (magenta) are observed in the subgranular zone (SGZ) and hilus. DAPI, nuclear staining; ML, molecular layer; GL, granular layer. (B) Pax6$^+$ cells co-express an early progenitor marker GFAP, neural stem cell markers nestin and Musashi1, and a late progenitor marker PSA-NCAM, but scarcely co-express a neuronal marker NeuN. Upper, GCL; under, Hilus. (C, C′) Morphological properties of Pax6$^+$ cells. (C) Many of Pax6$^+$ cells show radial glial shape and are often found in clusters in the SGZ. (C′) Pax6$^+$ cell has a GFAP$^+$ radial process. (D, D′, E, E′) Immuno-electron microscopy of Pax6$^+$ cells in the SGZ. P, Pax6$^+$ cells; G, granule cells; U, unknown cells. (D, E) Low magnification (× 1500) of Pax6$^+$ cells in the SGZ. (D′) High magnification (× 10 000) of Pax6$^+$ cell (magenta asterisk in D). Pax6$^+$ cell has irregular contours (magenta line, inset) and light cytoplasm containing a few ribosomes (r) and glial filaments (magenta arrows). Nuc, nucleus; mit, mitochondria. (E′) High magnification (× 5000) of Pax6$^+$ cell (yellow asterisk in E). Pax6$^+$ cells have smooth contours and dark scant cytoplasm negative for intermediate filaments.

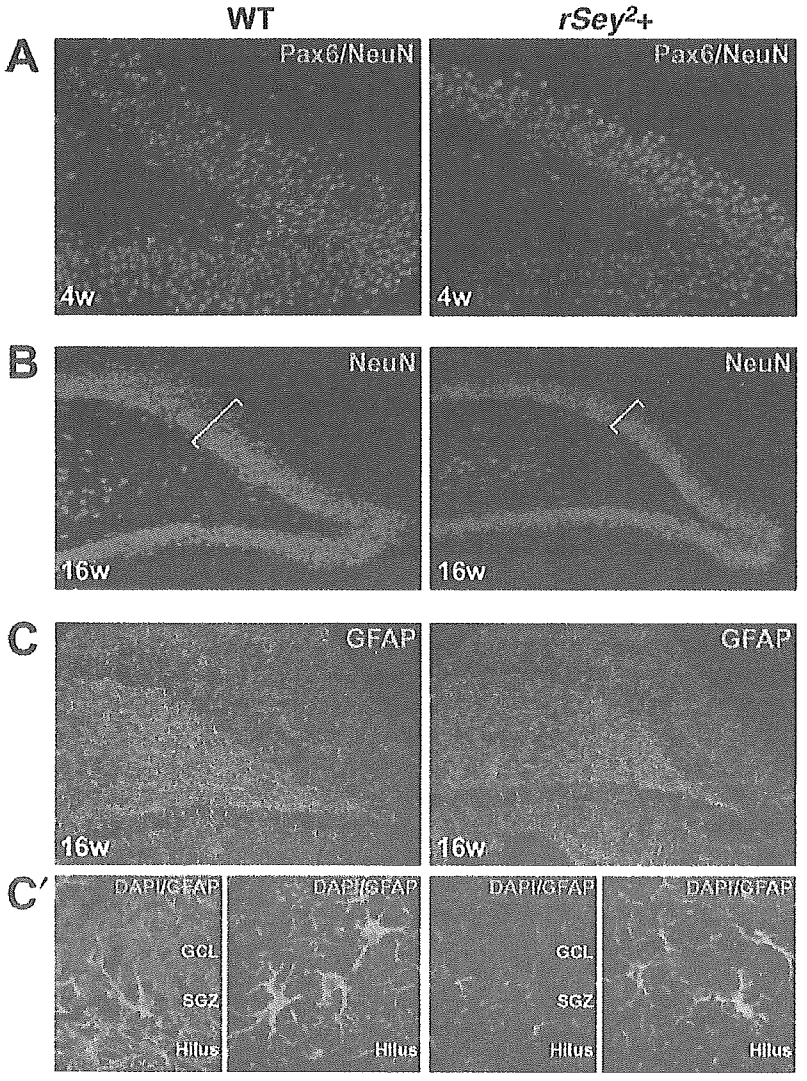

Figure 2 Morphologic defects in DG of *rSey*^{2}/+ rats. (A) In *rSey*^{2}/+ rats at 4 weeks, Pax6-expressing cells are less in number and the expression level of Pax6 is remarkably decreased. (B) In *rSey*^{2}/+ rats at 16 weeks, the thickness (bracket) of the granule cell layer (GCL) in the DG is thinner than that of WT. Granule cells are more packed in the GCL of *rSey*^{2}/+ rats compared with the WT. (C) The number of GFAP$^+$ cells is less in the DG of *rSey*^{2}/+ rats compared to WT. (C′) Radial glial fibers seem shorter and thinner in the DG of *rSey*^{2}/+.

rat (*rSey*^{2}). *rSey*^{2} is a spontaneous mutant that has a nonsense mutation in the *Pax6* gene (Osumi *et al.* 1997), although truncated Pax6 protein is undetectable in the homozygote (our unpublished observation). Since homozygous *Pax6* mutant rats die at birth, heterozygotes (*rSey*^{2}/+) were examined in this study. In the DG of *rSey*^{2}/+ at 4 weeks, we found that the number of Pax6$^+$ cells reduced and that an expression level of Pax6 also decreased (Fig. 2A). We could not observe an apparent difference in the architecture of the DG in *rSey*^{2}/+ rats at this stage.

At 16-week stage, we observed a prominent morphologic defect of the DG *rSey*^{2}/+ rats: the GCL was much thinner and the density of granule cells was higher in the DG of *rSey*^{2}/+ rats compared with the wild type (see brackets in Fig. 2B). We also noticed that the number of GFAP$^+$ cells was decreased and that the processes of GFAP$^+$ radial glial cells were thinner and underdeveloped in the DG of *rSey*^{2}/+ rats (Fig. 2C,C′). This may explain in part why granule cells were more packed in the DG of *rSey*^{2}/+ rats; there may be less spaces among granule cells because of thinner and underdeveloped radial glial processes. The previously mentioned character of Pax6-expressing cells in the DG of the wild type and the abnormalities in the DG of *rSey*^{2}/+ rats raised a possibility that the total number of new neurons in postnatal hippocampus is decreased in the haplo-insufficient condition of the *Pax6* gene.

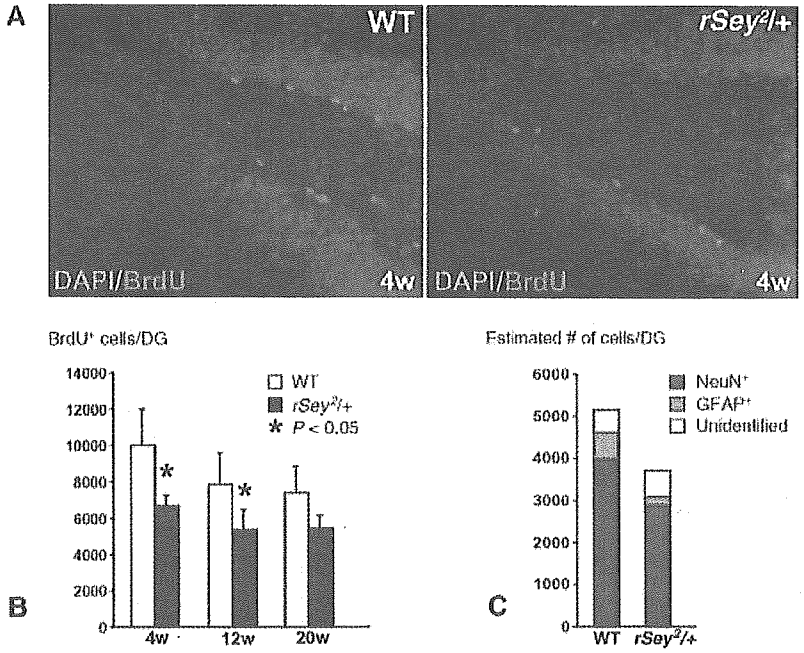

D

	BrdU⁺ cells			Developmental rate	
	12 week $n = 6$	12 + 4week $n = 3$	Survived	NeuN⁺ $n = 4$	GFAP⁺ $n = 4$
Wild type	7853 ± 1663	5160 ± 120.6	65.8 ± 0.1%	76.8 ± 8.2%	12.6 ± 1.3%
rSey²/+	5370 ± 1130	3712 ± 159.0	69.1 ± 0.1%	77.7 ± 6.9%	5.3 ± 1.0%

Table. Survival rate and developmental fates of BrdU⁺ cells in the dentate gyrus

Figure 3 Reduced cell proliferation and production of new neurons and astrocytes in the dentate gyrus of *rSey²/+* rats at postnatal stages. (A) The number of BrdU-positive cells (green) is decreased in the DG of *rSey²/+* rats after 3-day BrdU incorporation at 4 weeks. (B) The numbers of BrdU-positive cells within the DG are 33.3% ($P = 0.046$), 31.6% ($P = 0.021$), and 26.2% ($P = 0.051$) lower in the *rSey²/+* rats than in the wild-type at 4, 12, and 20 weeks, respectively. (C) Estimated numbers of cells double-positive for BrdU/NeuN (new neurons) and for BrdU/GFAP (new astroglia) based on the survival rate and the developmental fates shown in (D). Formation of new neurons and astroglia is markedly decreased in *rSey²/+* rats from 12 to 16 weeks. (D) Calculated survival rate and developmental fates of BrdU-positive cells in the DG 4 weeks after BrdU-injection at 12 weeks of age. The survival rate is not changed between WT and *rSey²/+*. In contrast, frequency of GFAP⁺ in total BrdU⁺ cells is less in *rSey²/+* at 4 weeks after BrdU injection, although that of frequency of NeuN⁺ in total BrdU⁺ cells is similar between WT and *rSey²/+* at 4 weeks after BrdU injection.

Decreased cell proliferation in the DG of *rSey²/+* rats

To address the question whether postnatal neurogenesis is affected in the SGZ of *Pax6*-deficient rats, we first compared the total number of BrdU⁺ cells in the DG between the wild type and *rSey²/+* at 4, 12, and 20 weeks. Rats were intraperitoneally injected with BrdU three times a day for 3 days and sacrificed at 24 h after the last BrdU injection (Kempermann & Gage 1999). In the DG of the wild type, the total number of BrdU-labeled cells in the SGZ per hemisphere decreased as the stage proceeded (Fig. 3A,B). Interestingly, a significant decrease in the total number of BrdU-labeled cells was observed in *rSey²/+* at 4 weeks (33.3% decrease), 12 weeks (31.6%), and 20 weeks (26.2%) (Fig. 3B). These data clearly indicate that the number of proliferating progenitor cells is considerably reduced in the SGZ of *Pax6*-deficient rat.

Next, we examined the fate of newborn cells in the DG. The wild type and *rSey²/+* rats were injected with BrdU three times a day for 3 days at 12 weeks and examined 4 weeks later based on the previous protocol (Kempermann & Gage 1999). Although the proliferating rate was much decreased in the DG of *rSey²/+* (Fig. 3B), there were no differences in the survival rate of newborn cells between the wild type and *rSey²/+* (Fig. 3D). The percentage of NeuN⁺ cells in total BrdU⁺ cells (new neurons) was also unchanged in *rSey²/+* (Fig. 3D). Contrastingly, the percentage of GFAP⁺ cells in total BrdU⁺ cells decreased to less than half in *rSey²/+* (Fig. 3D). This is superficially considered to be a reduction of newborn astrocytes. However, it is now widely accepted that GFAP⁺ astrocytes can serve as neural stem cells in the hippocampus (Seri *et al.* 2001). Eventually, the estimated total numbers of newly generated neurons and astrocytes/progenitor cells were dramatically reduced in the DG of *Pax6*-deficient rat (Fig. 3C).

In a BrdU labeling study for a longer period (2 weeks), the ratio of BrdU⁺/Pax6⁺ cells in the wild type was increased up to fivefold (35%) comparing with the samples labeled for a short period (30 min) (7.7% at 4 week; 6.3% at 6 week). This may imply that a population of cells expressing Pax6 contain neural stem cells (or quiescent GFAP⁺ early progenitor cells) whose cell cycle is longer than that of GFAP⁺ early progenitor cells. We also found

that the number of Pax6$^+$/GFAP$^+$ double-positive cells in *rSey*^{2}/+ was 22% less than that in the WT at 4 week (WT, 482 578 ± 33 757 cells/mm^3; *rSey*^{2}/+, 374 981 ± 21 527 cells/mm^3; $n = 4$, $P < 0.01$). Furthermore, the number of BrdU$^+$/Pax6$^+$ double-positive cells was 27% decreased in *rSey*^{2}/+ rats (WT, 238 208 ± 27 545 cells/mm^3; *rSey*^{2}/+, 174 921 ± 13 478 cells/mm^3; $n = 4$, $P < 0.01$) in BrdU labeling study for a longer period (2 weeks). All these results consistently suggest that Pax6 is essential for proliferation of neural progenitor cells, thereby keeping the size of the progenitor pool.

The number of GFAP$^+$ early progenitors decreased in the SGZ of *rSey*^{2}/+

To further elucidate the role of Pax6 in hippocampal neurognesis, we investigated at which step a transition of neurogenesis is impaired by detailed BrdU pulse/chase experiments combined with immunostaining with progenitor markers at 4 weeks. At the beginning, we re-examined the character of Pax6$^+$ cells in combination with BrdU labeling. Remarkably, more than 90% of total BrdU-incorporated cells in the SGZ expressed Pax6 at 30 min after BrdU injection (Fig. 4A,B). This result strongly suggests that Pax6 is vital for the cell proliferation in postnatal hippocampal neurogenesis. The fact that Pax6$^+$ cells are highly proliferative may also explain why they were often seen in clusters in the SGZ (Fig. 1A,C).

Then we investigated the cell-type transition of BrdU-incorporated cells in the SGZ of the wild-type and *Pax6*-deficient 4-week-old rats at 30 min, 24 h and 72 h after BrdU injection. In the wild type, the percentage of Pax6$^+$ cells in total BrdU$^+$ cells became markedly reduced from 30 min to 72 h, but 58% of BrdU$^+$ cells still expressed Pax6 at 72 h (Fig. 4B). The frequency of GFAP$^+$ in total BrdU$^+$ cells decreased between 30 min and 24 h after BrdU injection (Fig. 4C). Contrastingly, the ratio of PSA-NCAM$^+$ in total BrdU$^+$ cells increased between 30 min and 24 h after BrdU injection (Fig. 4D). These data are basically consistent with the results obtained in the mouse (Seri *et al.* 2001; Fukuda *et al.* 2003).

The same analyses were then performed on the DG of the *rSey*^{2}/+ rat. The percentage of Pax6$^+$ cells in total BrdU$^+$ cells slightly decreased but was statistically unchanged between the wild type and *rSey*^{2}/+ (Fig. 4B). In contrast, we found a significant decrease (38.4% decrease at 24 h; 49.6% decrease at 72 h, $P < 0.03$) in the frequency of GFAP$^+$ cells in total BrdU$^+$ cells (Fig. 4C) and an

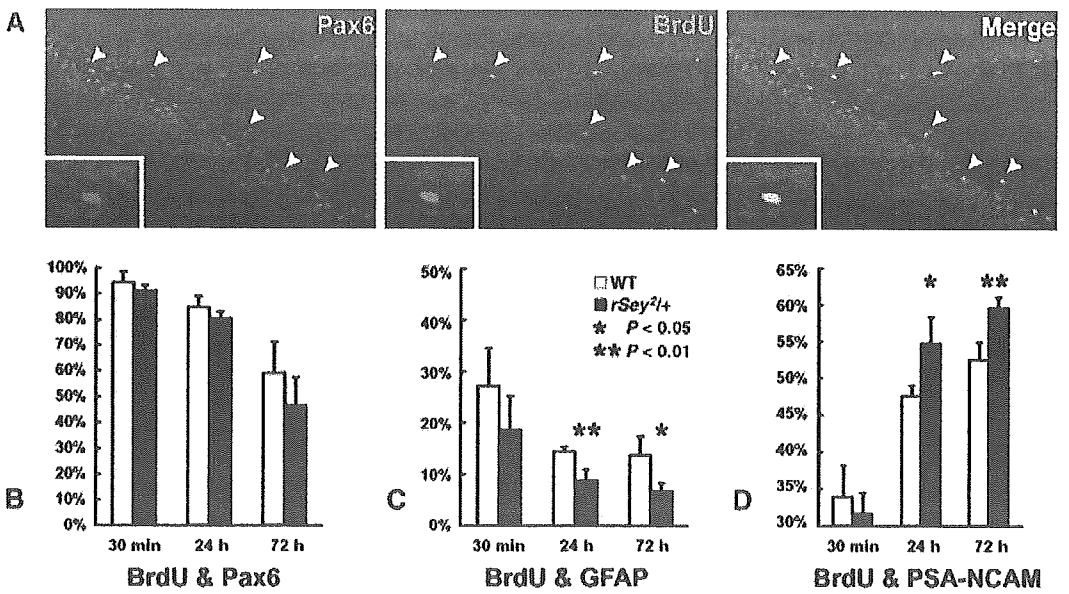

Figure 4 BrdU pulse/chase labeling assay in the DG of the 4-week-old wild type (WT) and Pax6 deficient (*rSey*^{2}/+) rats. (A) Confocal micrographs of BrdU-labeled Pax6$^+$ cells 30 min after BrdU injection. Most of BrdU labeled cells co-express Pax6 (arrows). In *rSey*^{2}/+, the expression level of Pax6 protein is reduced and the number of Pax6$^+$ cells is less than in the wild type. (B–D) Percentage of BrdU-labeled cells in the SGZ at 30 min, 24 h, and 72 h after BrdU injection. (B) At 30 min, more than 90% of BrdU$^+$ cells co-express Pax6. From 30 min to 72 h, the number of Pax6$^+$ cells becomes markedly reduced in WT and *rSey*^{2}/+. (C) Frequency of GFAP$^+$ in total BrdU$^+$ cells is less in *rSey*^{2}/+ at 24 h and 72 h after BrdU injection. (D) Contrastingly, more PSA-NCAM$^+$ cells are observed in total BrdU$^+$ cells in *rSey*^{2}/+ at 24 h and 72 h after BrdU injection.

opposite increase (15.1% increase at 24 h; 13.5% increase at 72 h, $P < 0.03$) in PSA-NCAM$^+$ cells (Fig. 4D). These data clearly indicate that maintenance of GFAP$^+$ early progenitor cells is extremely impaired in the DG of *rSey*^{2}/+.

We performed BrdU pulse labeling study with a short survival period (5 days) to examine whether Pax6 accelerates the neuronal differentiation from dividing PSA-NCAM$^+$ late progenitor cells to NeuN expressing immature neurons. The ratio of NeuN$^+$/BrdU$^+$ cells in this study was unchanged between WT and *rSey*^{2}/+ (4w WT, 63.4%; 4w *rSey*^{2}/+, 66.6%; $n = 4$, $P = 0.36$). Therefore, Pax6 may not be involved in neuronal differentiation but in maintenance of the GFAP$^+$ early progenitor cells by regulating their proliferation.

We further examined how the character of neural progenitors in the DG was different between the wild type and *rSey*^{2}/+ at 4 weeks. As described previously, 31.5% of Pax6$^+$ cells co-expressed a marker for the late progenitor, PSA-NCAM (Figs 1B and 5C). Quite interestingly, Pax6$^+$/PSA-NCAM$^+$ cells dramatically increased up to 55.5% in *rSey*^{2}/+ rats (45/81 cells; 76% increase than that of wild type; Fig. 5B,C). Moreover, GFAP and PSA-NCAM double-positive cells were scarcely detected in the DG of WT rats, while such GFAP$^+$/PSA-NCAM$^+$ cells were quite often observed in the DG of *rSey*^{2}/+ rats (Fig. 5D). These results may imply that premature neuronal differentiation occurs in the DG of the *rSey*^{2}/+. As seen in 16-week rats (Fig. 2C,C′), the number of GFAP$^+$ cells was much less in the SGZ and hilus, and GFAP$^+$ cells have thin and underdeveloped processes in *rSey*^{2}/+ rats (Fig. 5A,E). Quantitatively, the level of GFAP expression was 16% less in the mutant hippocampus as judged from real-time polymerase chain reaction (PCR) (data not shown). These results suggest that hippocampal neurogenesis is quite abnormal in *Pax6*-deficient rat. All the findings consistently suggest a pivotal role of Pax6 in maintenance of the GFAP$^+$ early progenitor cells in the postnatal hippocampus.

Wnt signaling is impaired in the DG of *rSey*^{2}/+

What kinds of molecules then regulate cell proliferation under the control of Pax6 transcription factor? Among various candidate factors, we focused on Wnt signaling molecules because their expressions are reported in the postnatal DG (Shimogori *et al.* 2004) and also because we ourselves have shown down-regulation of a Wnt ligand expression in *rSey*^{2}/*rSey*^{2} rat embryos (Osumi *et al.* 1997; Takahashi *et al.* 2002).

We first searched expression patterns of various Wnt signaling molecules by performing *in situ* hybridization of genes encoding Wnt ligands, Frizzled receptors, and a downstream molecule Dvl1. Among them, *Wnt7a*, *Wnt7b*, *Fz3*, and *Dvl1* showed interesting expression patterns in the DG for 3–4 weeks (Fig. 6). *Wnt7a*, a Wnt ligand, was preferentially expressed in the hilus and along the SGZ of the blades of the DG. Another Wnt ligand, *Wnt7b*, was detected in the SGZ and the GCL, but *Wnt7b*-expressing cells did not morphologically seem to be granule cells in the GCL. Weak expression of *Wnt3a* was also detected in the SGZ at 2 weeks, but almost diminished by 4 weeks in the rat (data not shown). These expression patterns of Wnt ligands hint us to imagine that they are expressed in the progenitors themselves or other cells that may constitute a niche for keeping the undifferentiated state of the progenitor cells. In the DG of *rSey*^{2}/+, the number of *Wnt7a*-expressing cells significantly decreased (687 cells in the wild type; 576 cells in *rSey*^{2}/+; 16% decrease), and the number of *Wnt7b*-expressing cells also decreased (607 in the wild type; 544 in *rSey*^{2}/+; 11% decrease). We could not observe any difference in expression of *Wnt3a* in the DG of *rSey*^{2}/+. Expression of a Wnt receptor *Fz3* was detected mainly in the GCL, and unchanged in the DG of *rSey*^{2}/+. Contrastingly, the expression level of *Dvl1* was increased in the DG of *rSey*^{2}/+ (Fig. 6). Taken altogether, Wnt signaling is impaired in the DG under the Pax6 deficient condition, which may result in reduced proliferation of GFAP$^+$ early progenitor cells in *rSey*^{2}/+.

Discussion

Pax6 expressed in GFAP$^+$ early progenitor cells in hippocampal neurogenesis

Previous papers suggest that adult hippocampal neurogenesis originates from precursor cells in the DG and results in new granule neurons through multiple steps from the GFAP$^+$ early progenitor cells to the PSA-NCAM$^+$ late progenitor cells (Seri *et al.* 2001; Fukuda *et al.* 2003; Kempermann *et al.* 2004). In the present study, we revealed that Pax6$^+$ cells frequently co-expressed GFAP and Musashi1, sometimes expressed nestin and PSA-NCAM, but scarcely co-expressed NeuN in the SGZ of the postnatal DG (Fig. 1B). That is, Pax6 is considered to be expressed mostly in the GFAP$^+$ early progenitor cells.

The ratio of nestin-positive cells among BrdU$^+$ was less than that in a previous study using nestin-EGFP reporter mice (Filippov *et al.* 2003; Fukuda *et al.* 2003). This may be due to difference in sensitivity of anti-nestin antibody and duration of nestin-promoter-driven EGFP. More importantly, a large number of Pax6$^+$/GFAP$^+$ cells had early progenitor-like morphology with a long radial